Nanoscale

REVIEW

View Article Online
View Journal | View Issue

Check for updates

Cite this: *Nanoscale*, 2024, **16**, 8196

Enzyme-mimic catalytic activities and biomedical applications of noble metal nanoclusters

Xinxin Pan,[a,b] Yidan Yao,[a,b] Manxi Zhang,[d] Xun Yuan,[c] Qiaofeng Yao *[a,b] and Wenping Hu[a,b]

Noble metal (*e.g.*, Au and Ag) nanoclusters (NCs), which exhibit structural complexity and hierarchy comparable to those of natural proteins, have been increasingly pursued in artificial enzyme research. The protein-like structure of metal NCs not only ensures enzyme-mimic catalytic activity, including peroxidase-, catalase-, and superoxide dismutase-mimic activities, but also affords an unprecedented opportunity to correlate the catalytic performance with the cluster structure at the molecular or atomic levels. In this review, we aim to summarize the recent progress in programming and demystify the enzyme-mimic catalytic activity of metal NCs, presenting the state-of-the-art understandings of the structure–property relationship of metal NC-based artificial enzymes. By leveraging on a concise anatomy of the hierarchical structure of noble metal NCs, we manage to unravel the structural origin of the catalytic performance of metal NCs. Noteworthily, it has been proven that the surface ligands and metal–ligand interface of metal NCs are instrumental in influencing enzyme-mimic catalytic activities. In addition to the structure–property correlation, we also discuss the synthetic methodologies feasible to tailoring the cluster structure at the atomic level. Prior to the closure of this review with our perspectives in noble metal NC-based artificial enzymes, we also exemplify the biomedical applications based on the enzyme-mimic catalysis of metal NCs with the theranostics of kidney injury, brain inflammation, and tumors. The fundamental and methodological advancements delineated in this review would be conducive to further development of metal NCs as an alternative family of artificial enzymes.

Received 19th January 2024,
Accepted 20th March 2024

DOI: 10.1039/d4nr00282b

rsc.li/nanoscale

Published on 21 maart 2024. Downloaded on 10/11/2024 6:49:01.

1. Introduction

Artificial enzymes, also known as enzyme mimics, have attracted increasing interest in the past half century since they were conceptualized in the 1970s[1] (Fig. 1). They heavily depend on synthetic organic[2] and inorganic materials[3] to recreate the catalytic activity and selectivity of natural enzymes. Inorganic nanoparticles, due to their stability and robustness in diverse catalytic scenarios, have emerged as one of the most investigated candidates of artificial enzymes, giving rise to nanozymes as an important subclass of artificial enzymes.[4,5] As briefly illustrated in Fig. 1, the concept of nanozymes was initially proposed in 2004.[6] In a seminal work by Gao *et al.* in 2007,[7] the peroxidase-like activity of Fe_3O_4 was recognized, paving an alternative avenue to deploy inorganic nanoparticles for mimicking the catalytic behaviour of diverse enzymes. Subsequently, considerable research efforts have been devoted to programming the structures of inorganic nanoparticles toward mimicking the structure and thus the catalytic per-

[a]*Key Laboratory of Organic Integrated Circuits, Ministry of Education & Tianjin Key Laboratory of Molecular Optoelectronic Sciences, Department of Chemistry, School of Science, Tianjin University, Tianjin 300072, China*
[b]*Collaborative Innovation Center of Chemical Science and Engineering (Tianjin), Tianjin 300072, China*
[c]*School of Materials Science and Engineering, Qingdao University of Science and Technology, Qingdao266042, China*
[d]*Joint School of National University of Singapore and Tianjin University International Campus of Tianjin University Binhai New City, Fuzhou 350207, P. R. China*

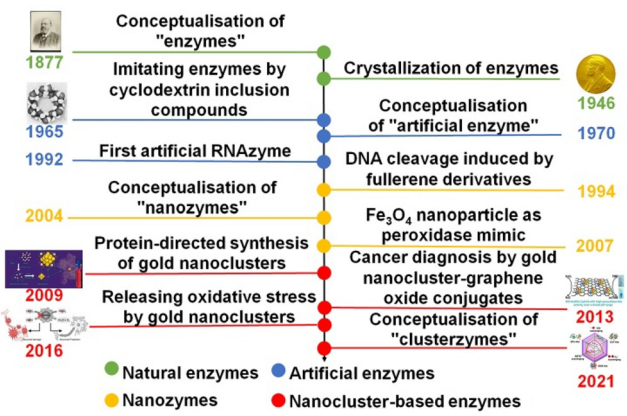

Fig. 1 A brief timeline for the development of artificial enzymes.

This journal is © The Royal Society of Chemistry 2024

Published on 21 maart 2024. Downloaded on 10/11/2024 6:49:01.

formance of natural enzymes.[8,9] For example, Xie *et al.* successfully synthesized gold NCs protected by bovine serum albumin (BSA) in 2009,[10] aiming to achieve synergism brought about by biomolecule–inorganic nanoparticle conjugation. Due to the intrinsic structural similarity between metal NCs and proteins, they have become intensively explored subclasses of artificial enzymes (*vide infra*), which were eventually termed "clusterzymes" in 2021.[11]

Noble metal (*e.g.*, Au and Ag) NCs are ultra-small nanoparticles with a core size of <3 nm.[12] They represent the transition state between single metal atom and crystalline nanometals, and usually could be descried by a definitive formula, *i.e.*, $[M_n(SR)_m]^q$, where n, m, and q are the numbers of metal (M), ligand (SR), and net charge of individual clusters, respectively.[13] The growing success of crystallography suggests that metal NCs feature a hierarchical structure reminiscent of biomolecules[14] (*e.g.*, proteins and DNAs), which ensures their feasibility in enzyme-mimic catalysis. In addition to the structural hierarchy, the accelerating development of advanced analytical techniques (including X-ray crystallography, X-ray absorption spectroscopy, and mass spectrometry) has allowed the geometric and electronic structures of metal NCs to be resolved at ~Å resolution,[15] which provides an unprecedented opportunity to establish a reliable relationship between the cluster structure and catalytic activity at the atomic level.[16] The combined structural hierarchy and atomic-level structural precision make metal NCs an ideal paradigm to design and study the enzyme-mimic catalytic performance of inorganic nanoparticles. For example, Liu *et al.* devised an artificial enzyme for relieving neuroinflammation based on 3-mercaptobenzoic acid (MPA)-protected Au_{25} NCs, exhibiting 137–160 times higher antioxidant activity than that of commonly used Trolox.[11] In a separate contribution, Shan *et al.* revealed the ligand effects of Au_{15} NCs on peroxidase-like activity, where *N*-acetyl-L-cysteine (NAC) ligands showed superior performance among the tested NAC, 3-mercapto-2-methylpropanoic acid (MMPA) and MPA due to their strong electron-withdrawing effect.[17]

Although encouraging achievements regarding the development of metal-NC-based artificial enzymes have been witnessed in the past decades,[18,19] there still exists a lack of a concise review systematically summarizing the emerging structure–property relationship of metal-NC-based artificial enzymes. Herein, we aim to address this gap based on a protein-like hierarchical structure model of thiolate-protected noble metal NCs, exemplifying the structural effects of metal NCs on their enzyme-mimic catalytic performance at the molecular and atomic levels. This review starts with an anatomy of metal NCs' structure by comparing it to that of natural protein, followed by a brief analysis of their impact on catalytic performance at the individual hierarchical level. Subsequently, the synthetic achievements making possible atom-level programming of metal NCs are reviewed. After the synthetic methodology, the topic comes to recent advances in the enzyme-mimic catalysis of metal NCs. Before concluding with our outlooks in this area, we also exemplify potential applications of the enzyme-mimic catalysis of metal NCs in the field of biomedicine.

2. Structure and synthesis of metal NCs

One of the most striking findings in the crystallography of noble metal NCs is their structural complexity and hierarchy comparable to those of natural proteins.[20–22] Such protein-like structural hierarchy has now been widely accepted as the origin of the enzyme-mimic catalytic activity and selectivity of metal NCs. In this section, the hierarchical structure of thiolate-protected noble metal NCs, together with their impact on catalytic performance, will be concisely discussed. We also manage to outline the synthetic strategies making the atomic-level modulation of cluster structures possible.

2.1 Structure of metal NCs

Thiolate-protected noble metal NCs possess a core–shell structure, where a M(0) core is wrapped by a monolayer of M(I)-SR motifs. Based on the structural components identified in this core–shell structural scheme (*e.g.*, M(0) core and M(I)-SR motifs), a structural hierarchy analogous to that of natural proteins can be sketched.[23] By taking the most explored

Xinxin Pan

Xinxin Pan received his B.S. (2020) and M.S. (2023) degrees under the supervision of Prof. Xun Yuan from Qingdao University of Science and Technology (QUST). He is currently a Ph.D. student under the supervision of Prof. Qiaofeng Yao at Tianjin university (TJU). His research interest mainly focuses on designing noble metal nanoclusters for biomedicine and catalysis.

Yidan Yao

Yidan Yao received her B.S. (2023) degree from Qingdao University of Science and Technology (QUST). She is currently a master student under the supervision of Prof. Qiaofeng Yao at Tianjin university (TJU). Her research interest mainly focuses on the catalytic applications of noble metal nanoclusters.

Published on 21 maart 2024. Downloaded on 10/11/2024 6:49:01.

$[Au_{25}(SR)_{18}]^-$ NCs as an example (Fig. 2), analogues to the types and numbers of amino acids, the types and numbers of metal atoms and thiolate ligands constitute the primary structure of metal NCs. The construction of secondary building blocks using metal atoms and thiolate ligands, *e.g.*, the icosahedral Au_{13} core and six units of the SR-[Au(I)-SR]$_2$ motifs of $[Au_{25}(SR)_{18}]^-$, gives rise to the secondary structure of metal NCs. The spatial arrangement of secondary building blocks can thus be regarded as the tertiary structure of metal NCs. For example, the symmetric arrangement of six SR-[Au(I)-SR]$_2$ motifs along the C_3 axis of the icosahedral Au_{13} core yields the complete structure of individual $[Au_{25}(SR)_{18}]^-$. Also analogous to natural proteins, the physicochemical properties, in particular the catalytic properties of metal NCs, are intricately governed by the hierarchical structure depicted above.

The primary structure of metal NCs can affect their catalytic performance essentially *via* two means, metal atoms and ligands (Fig. 2a). Metal atoms are commonly regarded as catalytically active centers in many reactions,[24] and it is believed that enhanced catalytic activity emerged in the nano-sized essentially stimulates enzyme-mimic catalytic activity of metal NCs.[25] As a good example, gold, being an inert metal at its bulk form, exhibits marked electrocatalytic and photocatalytic activities in many reactions, including the oxygen evolution reaction (OER),[26] the hydrogen evolution reaction (HER),[27–29] the carbon dioxide reduction reaction (CO_2RR)[30–36] and a couple of other organic reactions.[37,38] In 2010, positively charged gold nanoparticles were reported to possess intrinsic peroxidase-like activity, which were able to catalyze the oxidation reaction of 3,3,5,5-tetramethylbenzidine (TMB, a common peroxidase substrate) by H_2O_2 to develop a blue color in aqueous solution.[39] Subsequently, numerous studies have showcased the intrinsic enzyme-like catalytic activity of Au and its extensive utilization in diverse biomedical applications.[40] Beyond mono-metal NCs, the importance of metal atoms to the catalytic behavior of metal NCs can be clearly evidenced by the doping or alloying effects in bimetal or multi-metal NCs. As a good example, bimetallic Au/Pt NCs, produced by using engineered consensus tetrapeptide repeat (CTPR) protein modules as scaffolds in 2023, demonstrate enhanced peroxidase-mimic catalytic activity in comparison with the corresponding monometallic NCs (*i.e.*, Au NCs or Pt NCs protected by CTPR).[41] These Au/Pt NCs can be reused in multiple reaction cycles without significant loss of catalytic activity.

In addition to metal atoms, protecting ligands may play an equally important role in governing the catalytic performance of metal NCs. The catalytic activity can first be affected by the hydrocarbon structure of protecting ligands. For instance, Shan *et al.* synthesized Au_{15} NCs protected by thiolate ligands with varied hydrocarbon tails, which were evidenced crucial in dictating the affinity of the clusters toward H_2O_2. The authors proposed that the acetylamino group in NAC, with its electron-withdrawing effect, resulted in a lower electron density on Au atoms, leading to a significant enhancement of peroxidase-mimic catalytic activity (Fig. 3a).[17] Besides the hydrocarbon tails, coordinating atoms are crucially influential to the catalytic behavior of metal NCs. As a rule of thumb, the catalytic activity of P-coordinated Au and Ag NCs tends to be higher than that of S-coordinated ones, largely ascribed to the extraordinarily strong M–S bond (M = Au or Ag).[42] However, as a trade-off, the strong M–S bond can endow thiolate-protected Au/Ag NCs with improved stability, which is favorable for the construction of artificial enzymes.

Polyhedron-based M(0) core and M(I)-SR motifs constitute the basic building blocks of metal NCs (Fig. 2b), and therefore their structures are of central importance in dictating clusters' catalytic performance. To start with, the composition and structure of the M(0) core largely impact the electronic structure of metal NCs.[43–45] For instance, when a Pt atom is doped into the center of the Au_{13} core of $Au_{25}(SC_6H_{13})_{18}$, the electronic structure, which can be probed by the UV-visible-near-infrared (NIR) absorption spectrum, undergoes significant changes. The valence electron count of the cluster $N = n \times \nu_e - m - q$ varies from 8 of $[Au_{25}(SC_6H_{13})_{18}]^-$ to 6 of

Manxi Zhang

Manxi Zhang received his B.S. (2020) degree from Xiamen University (XMU). Then, he obtained his M.S. (2022) degree from the National University of Singapore (NUS). He is currently a Ph.D. student under the supervision of Prof. Jianping Xie at the Department of Chemical and Biomolecular Engineering, NUS. His research interest focuses on the self-assembly and crystallization of metal nanoclusters.

Xun Yuan

Xun Yuan received his B.E. (2006) and M.E. (2009) degrees from Shandong University of Technology, China, and Ph.D. degree (2014) from the National University of Singapore (NUS) under the supervision of Prof. Jianping Xie. After 3 years of his postdoctoral work at the Institute of Bioengineering and Nanotechnology (IBN), he joined Qingdao University of Science and Technology (QUST) as a professor in 2017. His research focuses on the synthesis and applications of metal nanoclusters.

This journal is © The Royal Society of Chemistry 2024

Published on 21 maart 2024. Downloaded on 10/11/2024 6:49:01.

$[PtAu_{24}(SC_6H_{13})_{18}]^0$ after doping with Pt, where ν_e is the valence electron count of M in $[M_n(SR)_m]^q$. This change results in the splitting of the 1p orbitals and the emergence of new bands at 1.1 eV (α) and 2.1 eV (γ) for $[PtAu_{24}]^0$, while the band at 1.8 eV (β) disappears[46] (Fig. 3b). Subsequent experiments have demonstrated that the altered electronic structure after Pt doping gives rise to enhanced catalytic activity in the HER.

The accessibility of the surface metal to reactants is a key factor that affects the catalytic performance in catalytic reactions. As M(I)-SR motifs determine the surface chemistry including the surface accessibility of metal NCs, they are crucially influential to catalytic properties. Such accessibility can be facilely varied by altering the length of the M–S bond. The Zhang group examined the enzyme-mimic catalytic activities of $Au_{24}Ag_1(MPA)_{18}$, $Au_{24}Cu_1(MPA)_{18}$, and $Au_{24}Cd_1(MPA)_{18}$ NCs (MPA = 3-mercaptobenzoic acid). Doping Ag into $Au_{25}(MPA)_{18}$ NCs resulted in a longer Ag–S bond (2.48 Å) than the pristine Au–S bond (2.36 Å). The enhanced accessibility brought about by such bond expansion gives rise to 72 times higher antioxidant activity than those of natural antioxidants.[47] Owing to similar bond length modulation, $Au_{24}Cu_1(MPA)_{18}$ and $Au_{24}Cd_1(MPA)_{18}$ NCs exhibit antioxidant capabilities that are 137 times and 160 times higher than that of Trolox, respectively. Moreover, $Au_{25}(MPA)_{18}$, $Au_{24}Cu_1(MPA)_{18}$, and $Au_{24}Cd_1(MPA)_{18}$ can also exhibit glutathione peroxidase (GPx-like), catalase-like, and superoxide dismutase-like activities, respectively.[11] In addition to the M–S bond, the types of M(I)-SR motifs can induce marked changes in the catalytic activity of metal NCs. Chen *et al.* reported a ligand-induced thermally reversible isomerization between two thiolate-protected 28-gold-atom NCs: $Au_{28}(S\text{-}c\text{-}C_6H_{11})_{20}$ (-c-C_6H_{11} = cyclohexyl) and $Au_{28}(SPh\text{-}^tBu)_{20}$ (-Ph-^{t}Bu = 4-*tert*-butylphenyl).[48] The crystallographic analysis suggests that both Au_{28} NCs adopt a face-centered-cubic (FCC) Au_{20} core, while $Au_{28}(S\text{-}c\text{-}C_6H_{11})_{20}$ NCs possess two trimeric SR-[Au(I)-SR]$_3$ and two dimeric SR-[Au(I)-SR]$_2$ motifs. In contrast, $Au_{28}(SPh\text{-}^tBu)_{20}$ NCs feature four dimeric SR-[Au(I)-SR]$_2$ motifs. By using catalytic CO oxidation as a probe reaction, it was observed that $Au_{28}(S\text{-}c\text{-}C_6H_{11})_{20}$ NCs exhibited higher catalytic activity for CO oxidation compared to $Au_{28}(SPh\text{-}^tBu)_{20}$ NCs. This difference in catalytic activity is likely due to more protruded protecting motifs of $Au_{28}(S\text{-}c\text{-}C_6H_{11})_{20}$ NCs that make the catalytically active Au(I) more accessible (Fig. 3c).

The three-dimensional arrangement of M(I)-SR motifs on the surface of M(0) core gives rise to a tertiary structure of metal NCs. Intriguingly, such spatial arrangement is capable of creating a pocket-like catalytic cavity resembling that observed in natural enzymes on the surface of metal NCs. For example, a pocket-like cavity formed by the arrangement of three SR-[Au(I)-SR]$_2$ motifs around a Au_3 facet of the Au_{13} core can be identified on the surface of $[Au_{25}(SR)_{18}]^-$ NCs (Fig. 2c). Nasaruddin *et al.* found that such a pocket-like cavity of $[Au_{25}(p\text{-}MBA)_{18}]^-$ NCs (*p*-MBA = *para*-mercaptobenzoic acid) was feasible to selectively co-adsorb two molecules of 4-nitrophenol and one molecule of BH_4^-, facilitating the reductive conjugation of 4-nitrophenol into 4,4′-dihydroxyazobenzene.[49] Of note, the spatial arrangement of M(I)-SR on the surface of the M(0) core can induce intrinsic chirality in metal NCs, bringing about stereoselectivity in asymmetric synthesis. Wang *et al.* conducted the synthesis of chiral $[Au_7Ag_8(dppf)_3(L\text{-}/D\text{-proline})_6](BF_4)_2$ (where dppf = 1,10-bis(diphenylphosphino) ferrocene) NCs and utilized them as catalysts for asymmetric Aldol reactions.[50] The authors revealed that L-/D-Au_7Ag_8 NCs exhibited not only marked enantioselectivity toward the β-hydroxy carbonyl product, but also significantly higher catalytic efficiency compared to pure ProAg or proline (ProAg was

Qiaofeng Yao

Qiaofeng Yao is currently a professor at the School of Science, Tianjin University. He received his B.S. degree from University of Science and Technology of China (2010) under the supervision of Prof. Shu-Hong Yu. He received his Ph.D. degree from the National University of Singapore (2015) under the joint supervision of Prof. Jianping Xie and Prof. Jim Yang Lee. He then carried out his postdoctoral research in the Prof. Jianping Xie group until 2021, when he was appointed as an associate professor at the Joint School of National University of Singapore and Tianjin University. He has become a full professor at Tianjin University since 2023. His research interest mainly focuses on the synthesis, self-assembly, and optoelectronic applications of atomically precise metal nanoclusters.

Wenping Hu

Wenping Hu is a professor at Tianjin University and a Cheung Kong professor of the Ministry of Education, China. He received his Ph.D. degree from the Institute of Chemistry, Chinese Academy of Sciences (ICCAS), in 1999. Then, he joined Osaka University and Stuttgart University as a research fellow of Japan Society for the Promotion of Sciences and Alexander von Humboldt, respectively. In 2003 he joined ICCAS as a full professor. He worked for Tianjin University in 2013 and was promoted to the vice president and deputy president of the university in 2016 and 2021, respectively. His research interest focuses on organic optoelectronics.

Published on 21 maart 2024. Downloaded on 10/11/2024 6:49:01.

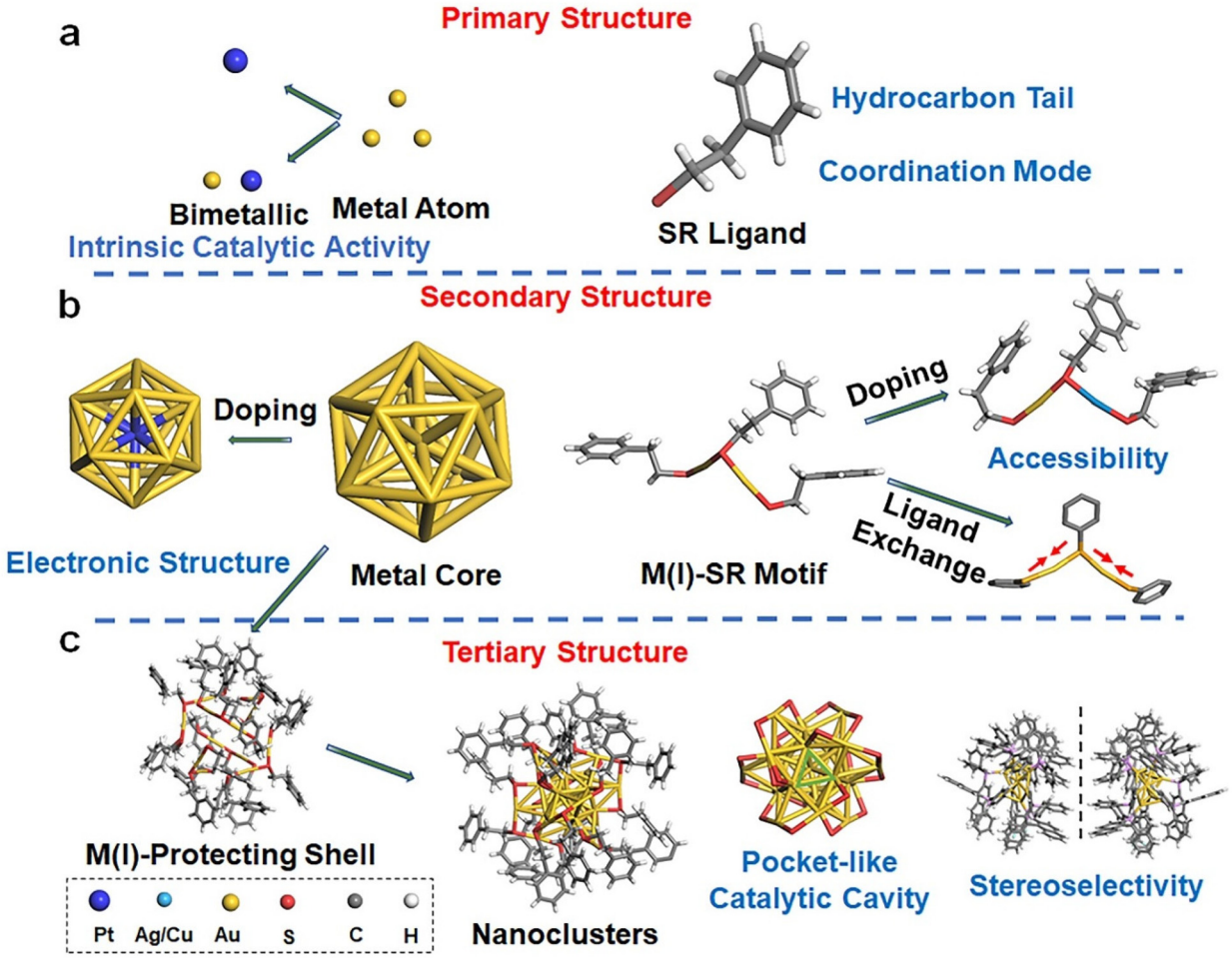

Fig. 2 Hierarchical structure of metal NCs and their contribution to the catalytic performance. The structure of NCs is exemplified by $[Au_{25}(SR)_{18}]^-$, where SR denotes the thiolate ligand. The numbers and types of metal atoms and ligands constitute the primary structure of metal NCs. The secondary structure modules formed by the aggregation of metal atoms and ligands, like Au(0) core and Au(I)-SR motifs, correspond to the secondary structure. The spatial arrangement of secondary structure modules then gives rise to the tertiary structure. The contributing factors to the catalytic performance at different structural hierarchies are shown in blue for easy identification.

synthesized by mixing $AgBF_4$ and proline). The improved catalytic activity can be attributed to the better accessibility to catalytically active sites afforded by the ordered arrangement of proline on the cluster surface (Fig. 3d).

2.2 Synthesis of metal NCs

Due to their molecule-like molecular formulas and properties, including HOMO–LUMO transitions,[51,52] strong luminescence,[53,54] and stereochemical activity,[55] metal NCs have long been regarded as metallic molecules.[56] Similar to organic molecules, they can be synthesized at atomic precision and with known step reaction pathways.[57,58] Until now, many synthetic methods have been documented to deliver the desired purity and quantity for selected metal NCs,[59–61] such as Brust-Schiffrin,[62] two-phase,[63] and seeded growth methods[64] and so on. These methods can be classified into three types: bottom-up synthesis, top-down synthesis, and inter-cluster conversion, according to the formation pathways of metal NCs.

2.2.1 Bottom-up synthesis. A bottom-up method, using Au NCs as an example, typically involves the chemical reduction of Au(I)–SR complexes, which can be facilely produced by mixing of Au(III) salt and thiolate ligands *via* the reaction of Au(III) + 3H-SR → Au(I)-SR + RS-SR + $3H^+$.[65] A series of reducing agents have been documented capable of partially reducing Au(I)–SR complexes to generate the Au(0) core, which is further capped by residual Au(I)–SR motifs to yield intact Au NCs.[66] Obviously, the choice of reducing agents is crucial in this process, and commonly used reducing agents can be categorized into two groups: (1) strong reducing agents such as $NaBH_4$ and (2) moderate or weak reducing agents like carbon monoxide (CO). When $NaBH_4$ is used as reducing agent, the formation process of Au NCs can be divided into two stages. The strong reducing power of $NaBH_4$ can first fuel a rapid reduction kinetics, generating a mixture of different-sized Au

 This journal is © The Royal Society of Chemistry 2024

Published on 21 maart 2024. Downloaded on 10/11/2024 6:49:01.

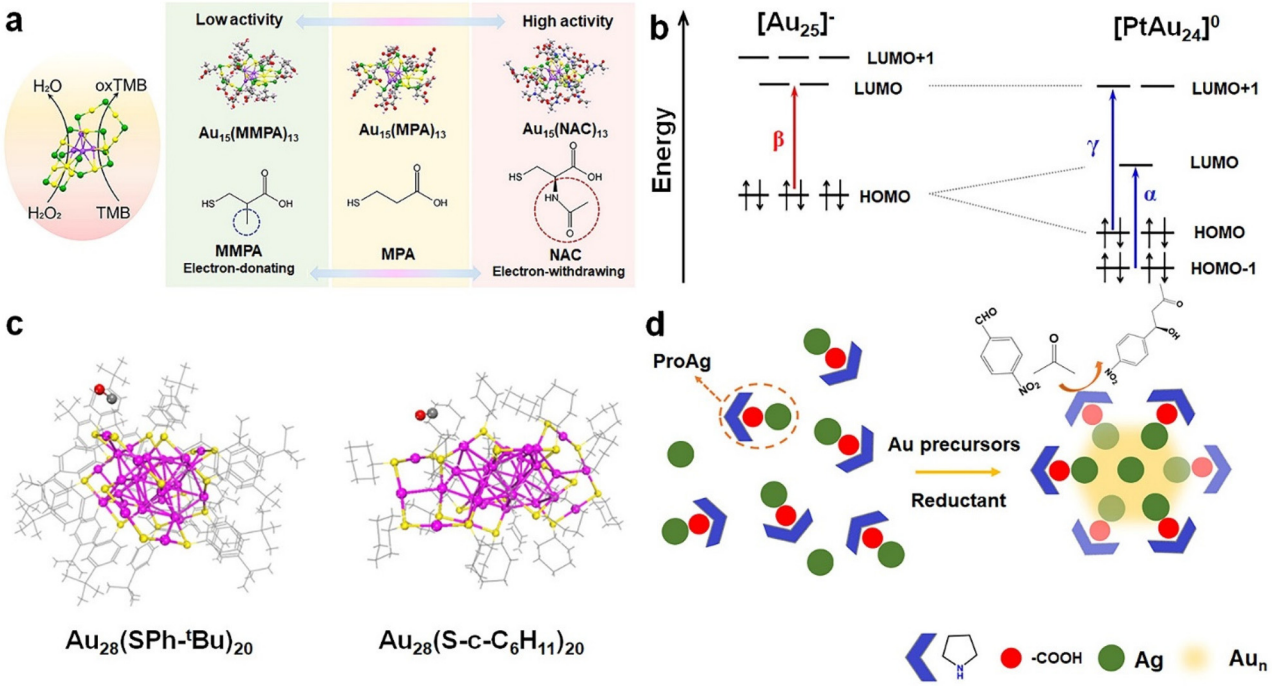

Fig. 3 (a) Schematic representation of the peroxidase-mimic activity of $Au_{15}(SR)_{13}$ NCs protected by different ligands. Reproduced from ref. 17 with permission from American Chemical Society, copyright 2023. (b) Electronic energy levels of $[Au_{25}(SC_6H_{13})_{18}]^-$ and $[PtAu_{24}(SC_6H_{13})_{18}]^0$. α, β, and γ denote the optical leaps of $[Au_{25}(SC_6H_{13})_{18}]^-$ and $[PtAu_{24}(SC_6H_{13})_{18}]^0$ at 1.1, 1.8, and 2.1 eV, respectively. Reproduced from ref. 46 with permission from Nature, copyright 2017. (c) Schematic representation of CO adsorption on the surface of two $Au_{28}(SR)_{20}$ cluster isomers. Reproduced from ref. 48 with permission from American Chemical Society, copyright 2016. (d) Schematic illustration of the stereoselective Aldol reaction catalyzed by L-/D-Au_7Ag_8 NCs. Reproduced from ref. 50 with permission from American Chemical Society, copyright 2023.

NCs. Following the fast reduction stage is a relatively slow size-focusing process, in which polydisperse Au NCs are converted into thermodynamically most stable size(s). It has now become clear that a balance between the fast reduction and slow size-focusing processes is a key to good controllability toward the structure attributes of Au NCs. More specifically, the relative time scale of the reduction and size-focusing kinetics, rather than their absolute time scale, dominates the monodispersity of the as-produced final Au NCs. As a good example, Yuan *et al.* carefully investigated the formation kinetics of Au NCs and devised a NaOH-mediated $NaBH_4$ method for the fast and high yield production of $[Au_{25}(SR)_{18}]^-$ NCs.[67] Introducing an aliquot amount of NaOH can simultaneously slow down the reduction kinetics and accelerate the size-focusing rate, sustaining a balance overall kinetics conducive to the formation of monodisperse Au_{25} NCs (Fig. 4a).

In comparison with $NaBH_4$, CO can maintain relatively mild reduction kinetics, suitable for kinetically trapping cluster growth into desired sizes. This is because the slow reduction kinetics makes the reduction reaction controllably quenchable at a selected stage, preventing clusters' further growth. In addition to the *in situ* size selection capability, the slow growth rate powered by CO reduction allows the formation process of metal NCs traceable *via* advanced mass spectrometry means. In 2014, Luo *et al.* employed electrospray ionization mass spectrometry (ESI-MS) to monitor the formation process of $[Au_{25}(SR)_{18}]^-$ in the presence of CO.[68] The detailed time-course ESI-MS analyses reveal 27 different Au(I)-SR complexes or intermediate cluster species, which can be represented by a general formula of $[Au_n(SR)_mCl_p]^q$. The most interesting finding is that all these $[Au_n(SR)_mCl_p]^q$ species possess an even-numbered valence electron count ($N = n - m - p - q$), implying that the size growth of Au NCs follows a two-electron (2 e^-) hopping mechanism. More specifically, Au NCs evolves in a valence electron sequence of 0 e^- → 2 e^- → 4 e^- → 6 e^- → 8 e^- → 10 e^-. A similar 2 e^- hopping mechanism has also been observed in the size growth reaction of $[Au_{44}(SR)_{26}]^{2-}$ mediated by $[Au_{25}(SR)_{18}]^-$. Yao *et al.* reduced Au(I)–SR complexes using CO in the presence of pre-formed $[Au_{25}(SR)_{18}]^-$, where the size growth reaction was monitored by time-course ESI-MS.[69] All 35 Au(I)–SR complex or intermediate cluster species identified in this process feature even-numbered valence electron counts, which evolves in a sequence of 2 e^- hopping. More intriguingly, successful capture of an adduct $[Au_{25}(SR)_{18}CO]^-$ by ESI-MS analysis indicates that the further growth of Au_{25} NCs is initiated by selective adsorption of CO on the cluster surface (Fig. 4b, top panel). Moreover, a careful analysis on the time-dependent abundance of intermediate species manifests two detailed growth pathways for the growth of $[Au_{25}(SR)_{18}]^-$ to $[Au_{44}(SR)_{26}]^{2-}$: monotonic LaMer-like growth or volcano-shaped aggregative growth (Fig. 4b, bottom panel).

Published on 21 maart 2024. Downloaded on 10/11/2024 6:49:01.

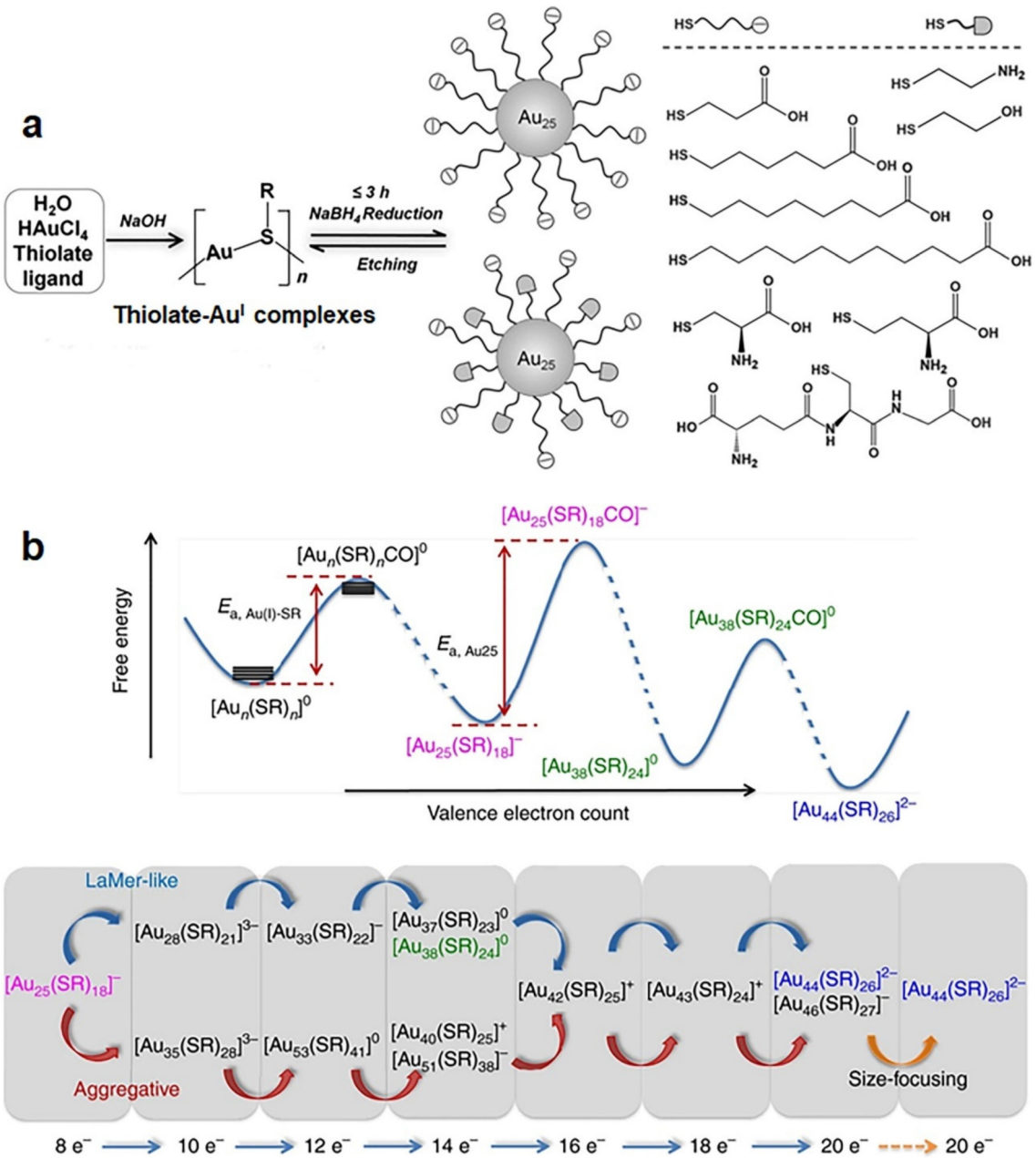

Fig. 4 (a) Schematic illustration of the NaOH-mediated $NaBH_4$ reduction method for the synthesis of $[Au_{25}(SR)_{18}]^-$ NCs with a broad library of thiolate ligands (shown in right). Reproduced from ref. 67 with permission from John Wiley and Sons, copyright 2014. (b) Schematic illustration of the CO-mediated size growth reaction from $[Au_{25}(SR)_{18}]^-$ to $[Au_{44}(SR)_{26}]^{2-}$. Reproduced from ref. 69 with permission from Nature, copyright 2017.

2.2.2 Top-down synthesis. In sharp contrast to the reduction growth in the bottom-up synthesis mentioned above, top-down synthesis depends dominantly on chemically etching larger-sized metal nanoparticles or NCs to generate smaller NCs.[70] The etching reaction is often driven by etching agents, of which the thiolate ligand is a good example, and highly dependent on the thermodynamic stability of clusters. Shichibu *et al.* reported the etching reaction of size-selected $Au_n(SG)_m$ (SG = glutathione) NCs with (n, m) = (10, 10), (15, 13), (18, 14), (22, 16), (25, 18), (29, 20), (33, 22), and (39, 24) using free GSH under aerobic conditions.[71] It is revealed that the $Au_n(SG)_m$ ($n < 25$) NCs are completely oxidized to Au(I)–SG complexes after 3 h reaction with GSH, while $Au_n(SG)_m$ ($n > 25$) NCs are focused into $Au_{25}(SG)_{18}$ (Fig. 5a). Based on such size-dependent stability in the etching reaction, the authors proposed a method for the large-scale synthesis of $Au_{25}(SR)_{18}$ NCs through thiol etching chemistry. To shed light on the etching chemistry of metal NCs at the molecular level, Cao *et al.* monitored the etching process of water-soluble $Au_{25}(SR)_{18}$ NCs in the presence of excess thiol ligands by real-time ESI-MS in a

 This journal is © The Royal Society of Chemistry 2024

Published on 21 maart 2024. Downloaded on 10/11/2024 6:49:01.

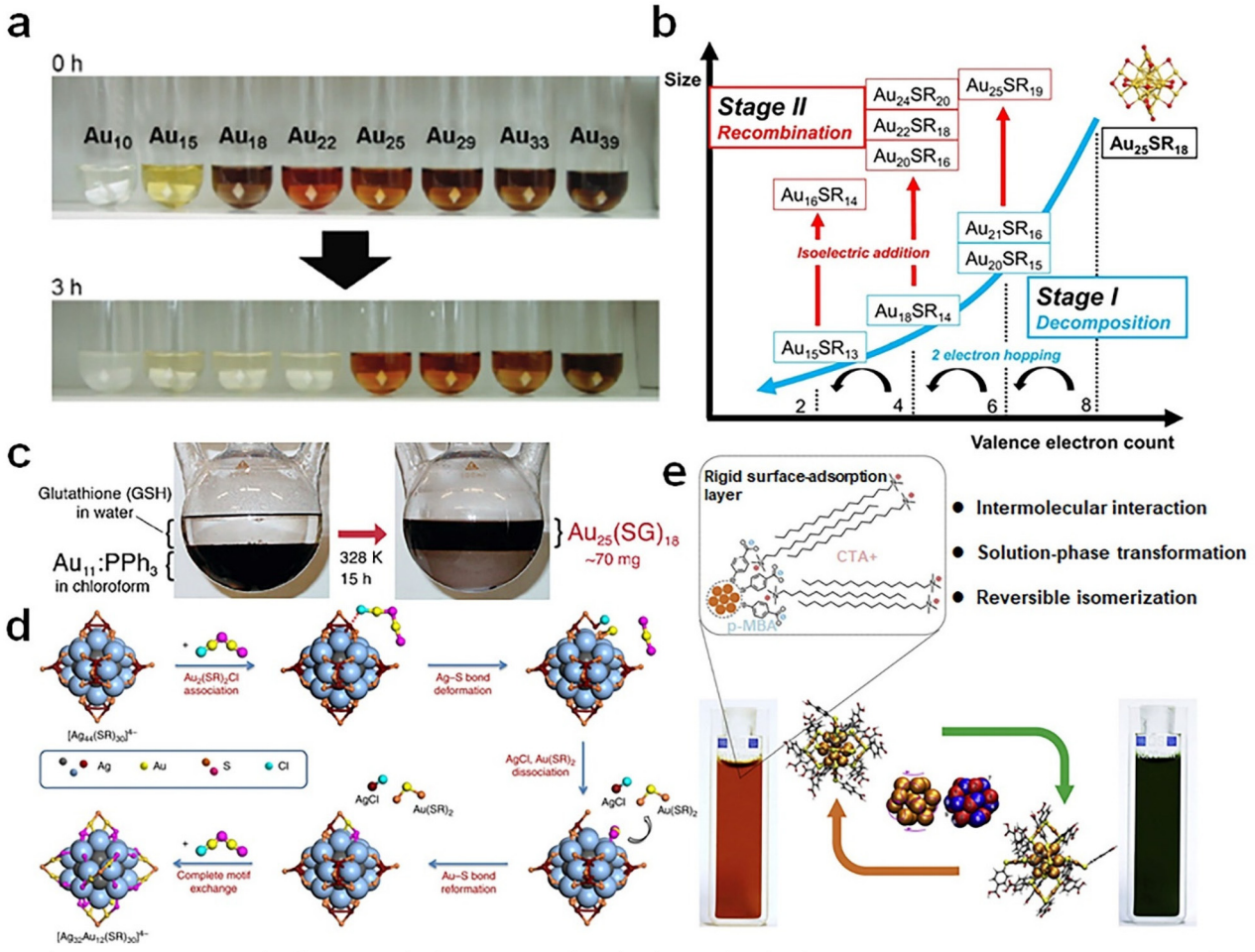

Fig. 5 (a) Aqueous solutions of different $Au_n(SG)_m$ clusters before (0 h) and after (3 h) the reaction with GSH. Reproduced from ref. 71 with permission from John Wiley and Sons, copyright 2007. (b) Schematic illustration of the etching reaction of water-soluble $Au_{25}(SR)_{18}$ using excess thiol ligands. Reproduced from ref. 72 with permission from Nature, copyright 2021. (c) Schematic diagram of ligand exchange-induced size conversion from $Au_{11}(PPh_3)_8Cl_3$ to $Au_{25}(SG)_{18}$. Reproduced from ref. 73 with permission from American Chemical Society, copyright 2005. (d) Schematic illustration of the surface motif exchange reaction of $[Ag_{44}(SR)_{30}]^{4-}$ NCs. Reproduced from ref. 75 with permission from Nature, copyright 2017. (e) Schematic representation of the reversible transformation between the two isomers of $[Au_{25}(p\text{-MBA})_{18}]^-$ NCs using a cationic surfactant (cetyltrimethylammonium cation, CTA^+). Reproduced from ref. 76 with permission from Cell, copyright 2021.

course of 30 days[72] (Fig. 5b). Intriguingly, the authors identified several NC species that were not observed in the bottom-up growth process of $Au_{25}(SR)_{18}$. The authors thus rationalized that these species should be formed by the recombination of Au(I)–SR complexes with *in situ* generated $Au_n(SR)_m$ species by the etching reaction. Such molecular insights into the etching reaction also offers an alternative strategy to produce novel sizes not found in bottom-up growth reactions.

2.2.3 Inter-cluster conversion. The inter-cluster conversion method uses pre-formed metal NCs as precursors and leverages on their reactions induced by chemical (*e.g.*, oxidizing/reducing agents and ligands) and physical (*e.g.*, solvent polarity and temperature) stimuli. When foreign ligands are used as stimuli, they often induce ligand exchange reactions, which may or may not be accompanied by size conversion dependent on the nature of pristine and foreign ligands. A good example for the ligand exchange-induced size conversion reaction is the production of $Au_{25}(SG)_{18}$ NCs from $Au_{11}(PPh_3)_8Cl_3$ NCs, where PPh_3 is triphenylphosphine.[73] As shown in Fig. 5c, reacting hydrophobic $Au_{11}(PPh_3)_8Cl_3$ NCs (in chloroform) with excess GSH molecules can convert the cluster size into $Au_{25}(SG)_{18}$, whose good hydrophilicity can simultaneously induce a phase-transfer reaction into the water phase. Besides the size conversion reaction, size-maintained ligand exchange reactions have been extensively documented. For instance, by reacting water-soluble $[Ag_{44}(MNBA)_{30}]^{4-}$ (MNBA = 5-mercapto-2-nitrobenzoic acid) with a series of organo-soluble thiolate ligands like 4-fluorothiophenol (4-FTP), 4-nitrothiophenol (4-NTP), and 2-naphthalenethiol (2-NT), the cluster can undergo complete ligand exchange while maintaining the size unchanged.[74] In addition to ligand exchange, the inter-cluster transition reaction can be driven by the motif exchange mechanism. As shown in Fig. 5d, the reaction of $[Ag_{44}(SR)_{30}]^{4-}$ with $[Au_2(SR')_2Cl]^-$ complexes,[75] where

Published on 21 maart 2024. Downloaded on 10/11/2024 6:49:01.

SR′ denotes the incoming thiolate ligand, can induce the exchange of surface $Ag(SR)_2$ with $Au(SR')_2$, leading to the formation of $[Ag_{43}Au(SR)_{28}(SR')_2]^{4-}$. Upon sufficient supply of $[Au_2(SR')_2Cl]^-$, all 12 Ag atoms in the protecting motifs of $[Ag_{44}(SR)_{30}]^{4-}$ can be replaced by Au heteroatoms, giving rise to $[Ag_{32}Au_{12}(SR)_6(SR')_{24}]^{4-}$.

Isomerization may represent the most delicate means for modulating the cluster structure without altering its chemical composition (*i.e.*, formula). It is attracting recent research interest as it holds an unprecedented opportunity to decouple the size and structure effects in the structure–property relationship investigation of metal NCs. As an illustrative example, Cao *et al.* made full use of CH···π interactions between cetyltrimethylammonium (CTA^+) cations and *p*-MBA ligands, a bilayer of CTA^+ cations can be coated on the surface of $[Au_{25}(p\text{-}MBA)_{18}]^-$ NCs[76] (Fig. 5e). Intriguingly, such surface modification can induce the core structure transformation of $[Au_{25}(p\text{-}MBA)_{18}]^-$, where a rotation of Au_{13} core is noted. In this way, a topological isomer of $[Au_{25}(p\text{-}MBA)_{18}]^-$ (denoted as $[Au_{25}]_G$ against the pristine $[Au_{25}]_R$ isomer) can be constructed without breaking any Au–S bond. More importantly, this isomerization process was evidenced reversible when the CTA^+ cations were removed from cluster surface.

3. Enzyme-mimic catalytic activity of metal NCs

Due to their protein-like hierarchical structure, together with the established methodology for customizing the property-dictating structure attributes at the atomic level,[77] metal NCs have been demonstrated with catalytic activities resembling those of natural enzymes. In this section, the enzyme-mimic catalytic performance of metal NCs will be briefly reviewed with an emphasis on their underlying chemistry.

3.1 Peroxidase-mimic catalytic activity

Peroxidase (POD) is a kind of natural enzyme that catalyzes the decomposition of H_2O_2 into hydroxyl radicals ($^{\bullet}OH$) and H_2O.[78] Subsequently, the as-generated $^{\bullet}OH$ oxidize the substrate, serving as the fundamental principle for numerous detection applications. In 2010, positively-charged gold nanoparticles were reported to possess intrinsic POD-like activity,[39] catalyzing the oxidation of TMB by H_2O_2. The as-obtained oxidation product, oxTMB, is blue in aqueous solution, offering a good chromogenic mechanism for probing $^{\bullet}OH$. In a subsequent study, Wang *et al.* investigated the surface effects of gold nanoparticles on their POD-like catalytic activity.[79] They compared the enzyme-mimic catalytic activity of unmodified, amino-modified, and citrate-capped gold nanoparticles toward the oxidation reaction of H_2O_2. Interestingly, they found that unmodified gold nanoparticles exhibited significantly higher enzyme-mimic catalytic activity towards POD the substrate.[79] This suggests that the superficial gold atoms play an important role in the POD-like catalysis.

The mechanism of the POD-mimic activity of Au nanoparticles was investigated by Li *et al.* They suggest that both POD-like activity and their pH-switchability are the intrinsic properties of metal atoms, regardless of the surfaces and intersections of facets exposed to environments.[80] More specifically, the adsorbed H_2O_2 molecule can undergo two types of decompositions:

acid-like decomposition:

$$H_2O_2* \leftrightarrow H* + HO_2* \quad (1)$$

base-like decomposition:

$$H_2O_2* \leftrightarrow H_2O* + O* \quad (2)$$

where the asterisk (*) is used to mark species absorbed on metal surfaces. The authors then indicate that the base-like decomposition yielding H_2O^* and O^* is more favorable under neutral conditions, while the acid-like decomposition hardly occurs because of its high energy barrier (Fig. 6a). Subsequently, the decomposition pathways with pre-adsorbed H and OH were studied to understand the origin of the pH dependency in the decomposition reaction of H_2O_2 on the Au (111) surface. As H_2O_2 prefers base-like decomposition under neutral conditions, the pre-absorbed H has little influence on H_2O_2 decomposition (eqn (3)). This reaction has a higher energy barrier than that for the direct decomposition of $H_2O_2^*$ to $2OH^*$.

$$H* + H_2O_2* \leftrightarrow H_2O* + OH* \quad (3)$$

However, when H_2O_2 adopts the base-like decomposition pathway under acidic conditions, it gives rise to OH^* and subsequently H_2O^* and O^* as products (Fig. 6b). The generated O^* is highly oxidizable and will readily abstract hydrogen atoms from organic substrates. These results suggest that the Au surface can exert stronger POD-mimic catalytic activity under acidic conditions, which catalyzes the oxidation of organic substrates in the presence of H_2O_2. This mechanism is applicable to various metals, including Au, Ag, Pt, and so on.

The metal surface-mediated catalytic mechanism remains valid for metal NCs, and metal NCs tend to exhibit higher catalytic activity due to their larger surface-to-volume ratio. Jiang *et al.* discovered that apoferritin-paired Au NCs (Au-Ft) have even higher activity at near acidic pH compared to native enzymes.[81] The improved stability of Au-Ft also endows them with a broader operation temperature window. It is not only Au NCs that possess good catalytic activity by mimicking PODs, but also the NCs of other metals like Cu, Pt, *etc.* which show similar POD-mimic catalytic activity. For instance, Jin *et al.* utilized yeast extract as a reducing agent and stabilizer to prepare Pt NCs through a one-step method.[82] These Pt NCs can effectively catalyze the oxidation of TMB in the presence of H_2O_2. Analysis of the catalytic mechanism suggests that such efficient POD-like activity may arise from electron transfer between TMB and H_2O_2 accelerated by Pt NCs. Maity *et al.* synthesized Cu NCs using pepsin as a template. The as-obtained Cu NCs, denoted as Cu_{23}@pepsin, consist of 23 Cu atoms

 This journal is © The Royal Society of Chemistry 2024

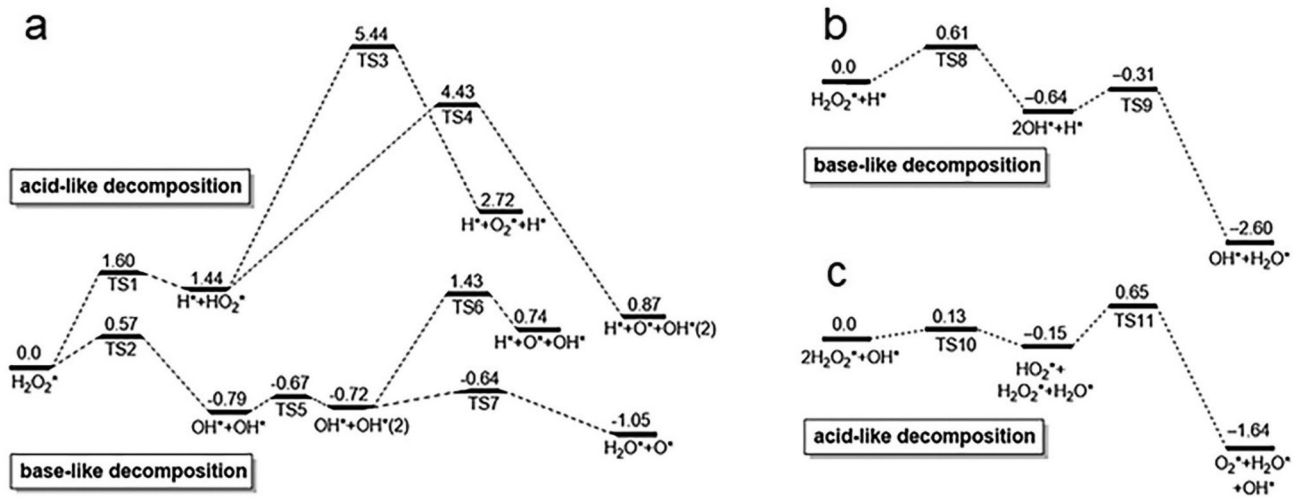

Fig. 6 Calculated reaction energy profiles for H_2O_2 decomposition on the Au (111) surface under (a) neutral, (b) acidic, and (c) basic conditions. TS1–11 represent the intermediate states of H_2O_2 adsorption and decomposition under different conditions, respectively. Reproduced from ref. 80 with permission from Elsevier Sci Ltd, copyright 2015.

Published on 21 maart 2024. Downloaded on 10/11/2024 6:49:01.

within a pepsin molecule and exhibit strong blue luminescence at 455 nm.[83] Cu_{23}@pepsin demonstrates high activity in catalyzing the reduction of H_2O_2 and the oxidation of *o*-phenylenediamine (OPD) according to the Michaelis–Menten enzyme kinetics.

Recent advancements in doping or alloying chemistry have offered a simple and effective means for enhancing the catalytic activity of metal NCs, making many doped or alloy NCs more effective in mimicking enzymes compared to monometal NCs. For instance, Mora-Sanz *et al.* have developed gold–platinum bimetallic NCs within the immunoglobulin G (IgG) structure (denoted as Au/Pt NCs-IgG hereafter).[84] The presence of two different types of metal atoms in these NCs leads to a synergistic effect, resulting in higher catalytic activity compared to the corresponding mono-metal NCs. However, it is worth noting that metal NC-based artificial enzymes generally exhibit poor pH tolerability, stimulating numerous studies aiming to structural and catalytic stability across a wide range of pH values. Tao *et al.* achieved this by adsorbing Au NCs onto graphene oxide through electrostatic interactions, resulting in the formation of synergistic GO–Au NC hybrids with exceptional POD-like activity[85] (Fig. 7a–c). Remarkably, the GO–Au NC hybrids exhibit marked catalytic activity over a broad pH range of 3–7 (Fig. 7d). Kinetic analysis reveals that the activity of the GO–Au NC hybrids at neutral pH is comparable to that of natural horseradish peroxidase (HRP) under the same conditions.

In addition to the improved ratio of surface metal atoms, the large surface-to-volume ratio of metal NCs leads to enhanced ligand effects on the catalytic activity of metal NCs. Recent studies have indicated that passivating ligands on the surface of metal NCs can restrict the accessibility of Au NCs to the reaction substrate. Therefore, in many cases, removal or partial removal of protecting ligands can increase the catalytic activity of metal NCs by promoting the exposure of surface metal atoms. For example, by hydrolyzing the BSA ligands on the surface of BSA–Au NCs using trypsin, a greater number of active sites on the BSA–Au NCs are exposed, resulting in an increased enzyme-mimic catalytic activity.[86] However, it should be mentioned that sufficient ligands are typically required to stabilize the structure of metal NCs, preventing their size change that can significantly hamper the investigation of structure–property relationship.

3.2 Catalase-mimic catalytic activity

Catalase (CAT) is a naturally occurring enzyme that catalyzes the production of O_2 and H_2O from H_2O_2.[87] The catalytic mechanism involves OH pre-adsorption under basic conditions, where H_2O_2 transfers an H* to the pre-adsorbed OH, resulting in the formation of HO_2* and H_2O*. Subsequently, HO_2* reacts with another H to generate H_2O_2*, ultimately giving rise to H_2O* and O_2* (Fig. 6c).[80] In the original study, it was demonstrated that Au nanoparticles possess the ability to quench $^{\bullet}OH$ and $O_2^{\bullet-}$.[88] Subsequent studies discovered that bimetallic AuPt nanoparticles protected by pectin, which were synthesized through citric acid reduction, exhibited superior CAT activity, particularly when the content of Pt was over 50%.[89] This suggests that doping is an effective approach to enhance the CAT-like activity of metal NCs. Ma *et al.* demonstrated that doping a single Cu heteroatom into Au_{22} NCs was able to remarkably enhance clusters' CAT-like activity[90] (Fig. 7g). The CAT-like activity of the prepared $Au_{21}Cu_1(SG)_{18}$ NCs was found 90 times higher than that of pristine $Au_{22}(SG)_{18}$ NCs. Such enhancement in activity was attributed to the reduction of the band gap from 1.33 eV to 1.28 eV through the doping of a single Cu heteroatom. The same group has also doped $Au_{25}(SG)_{18}$ NCs with Cu and Pt to form $Au_{24}Cu_1(SG)_{18}$ and $Au_{24}Pt_1(SG)_{18}$,[11,91] respectively, in which

Published on 21 maart 2024. Downloaded on 10/11/2024 6:49:01.

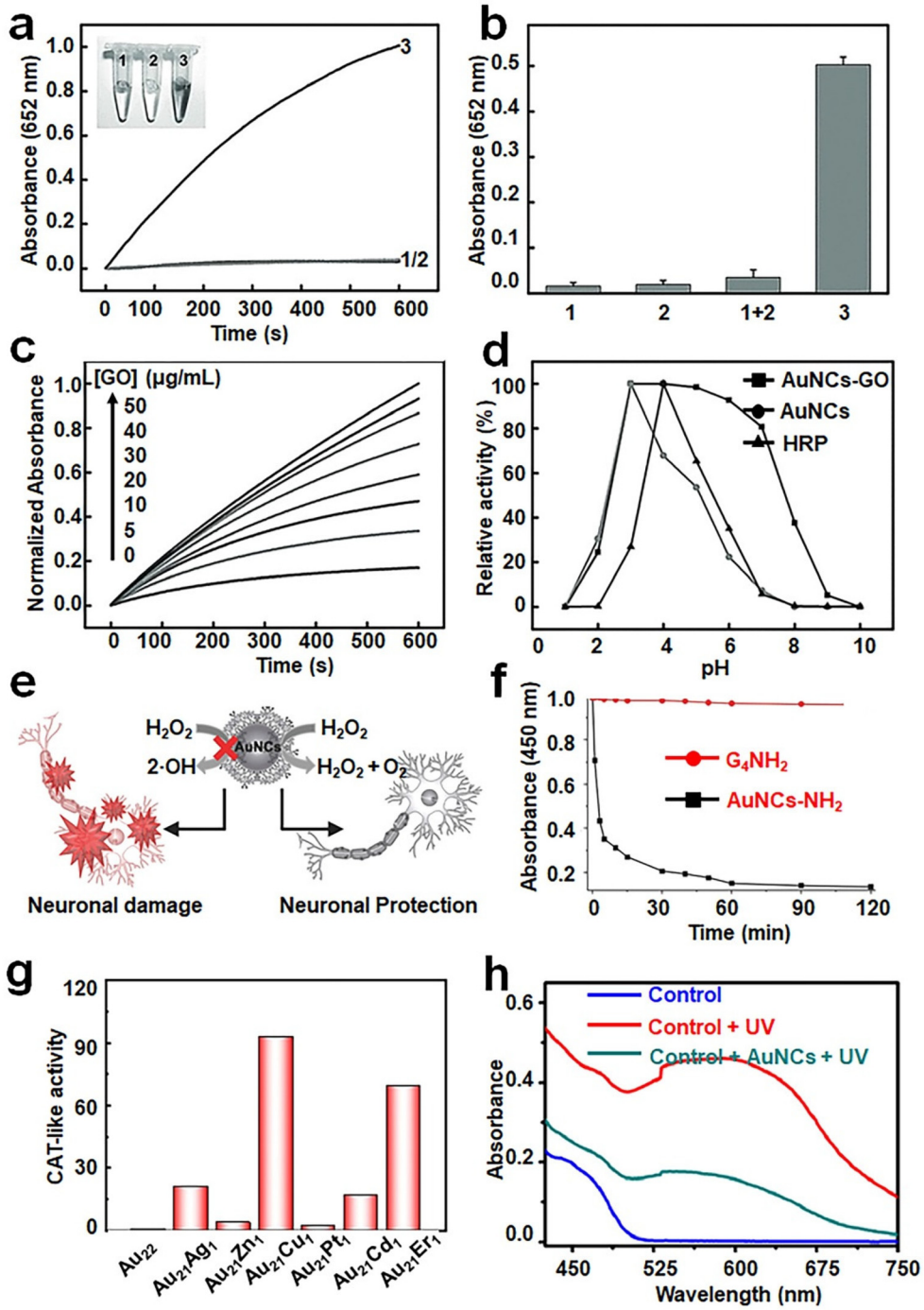

Fig. 7 (a) Time-dependent absorbance changes of TMB solution at 652 nm in the presence of GO (1), Au NCs (2) and the GO–Au NC hybrid (3) in phosphate buffer. (b) Absorbance values at 652 nm after 600 s. (c) Time-dependent absorbance changes at 652 nm of TMB reaction solutions catalyzed by the GO–Au NC hybrid at different concentrations of GO in phosphate buffer. (d) pH dependence of the POD-like activity of the GO–Au NC hybrid. Reproduced from ref. 85 with permission from John Wiley and Sons, copyright 2013. (e) Schematic diagram showing the dendrimer-encapsulated Au NCs with CAT-like activity for primary neuronal protection against oxidative damage. (f) Examination of the CAT-like activity of Au NC-NH_2. Reproduced from ref. 94 with permission from John Wiley and Sons, copyright 2016. (g) Diagram of the CAT-like activity of $Au_{22}(SG)_{18}$ and $Au_{21}M_1(SG)_{18}$ NCs. Reproduced from ref. 90 with permission from Science, copyright 2023. (h) SOD-like activity of CS-GSH@Au NCs by the NBT (*p*-nitro-blue tetrazolium chloride) chromogenic method. Reproduced from ref. 99 with permission from Elsevier Sci Ltd, copyright 2021.

enhanced CAT-like activities were recorded on the alloy NCs. In contrast, Hua *et al.* synthesized atomically precise $Pt_2M_4(C_{21}H_{27}O_2)_8$ NCs (M = Au, Ag, and Cu), among which only $Pt_2Au_4(C_{21}H_{27}O_2)_8$ exhibited CAT-like activity ($C_{21}H_{27}O_2$ = levonorgestrel).[92] These findings demonstrate that the doping of Au significantly increases its CAT activity compared to the

 This journal is © The Royal Society of Chemistry 2024

Published on 21 maart 2024. Downloaded on 10/11/2024 6:49:01.

doping of Cu and Ag. The reason for this may be the lower valence band energy of $Pt_2Au_4(C_{21}H_{27}O_2)_8$ relative to those of $Pt_2Ag_4(C_{21}H_{27}O_2)_8$ and $Pt_2Cu_4(C_{21}H_{27}O_2)_8$. Therefore, it has become clear that selecting more active metals is a promising approach to enhance the CAT-like activity of metal NCs, as long as the stability issue of the as-prepared NCs can be addressed. As another good example, by using cysteamine as a template agent and hydrazine hydrate as a reducing agent,[93] a simple, green method has been developed to synthesize monodisperse Cu NCs with excellent CAT-like activity.

In addition to the impact of metal atoms, surface ligands play an indispensable role in dictating the CAT-like activity of metal NCs. As a notable example, Liu *et al.* successfully synthesized aminated macromolecule-encapsulated Au NCs (Au NCs-NH_2) using a one-step process.[94] Fig. 7e provides a schematic diagram illustrating the enzymatic activity of Au NCs-NH_2, which has good potential in mitigating antioxidant damage in primary neurons. The mitigating effect is primarily attributed to the CAT-like activity of Au NCs-NH_2 that catalyze the production of O_2 from H_2O_2 (Fig. 7f). It should also be spotted out that conjugating the cluster surface with small molecules with intrinsic anti-oxidizing activity, of which *N*-acetylcysteine is a good example, may introduce additional anti-oxidizing activity to NCs. In this way, surface modification has been carried out on Au NCs for realizing their potential applications in acute kidney injury treatment.[95] Other than intrinsic activities brought about by the ligands, the ionization of the surface ligand may affect the pH of the solution, thereby influencing the CAT-like activity of the corresponding metal NCs. For instance, ultra-small Au NCs grafted with indocyanine green (ICG) exhibit strong CAT-like catalytic activity due to the presence of amino groups on their surfaces, which helps in maintaining a neutral pH in the solution.[96]

3.3 Superoxide dismutase-mimic catalytic activity

Superoxide dismutase (SOD), a metalloenzyme, plays a crucial role in catalyzing the disproportionation of superoxide anion radicals ($O_2^{\bullet-}$) into H_2O_2 and molecular O_2.[97] Initially, Pt nanoparticles were utilized as an effective material for eliminating $O_2^{\bullet-}$, followed by the successful elimination of $O_2^{\bullet-}$ by Pt-doped (with various doping contents) Au nanoparticles.[98] In a subsequent contribution by Liu *et al.*, Cu NCs were also found to possess significant SOD-like activity.[93] Similar to POD-like and CAT-like activities, the SOD-like activity of atomically precise Au NCs can be significantly enhanced by Cu or Pt heteroatom doping. Therefore, atomic-scale doping serves as an effective method for modifying the SOD-like activity of metal NCs.

The design of surface ligands can also contribute to modulating the SOD-like activity of metal NCs. For instance, Mi *et al.* successfully synthesized red-emitting CS–GSH@Au NCs, where CS denotes chitosan in HeLa cells by using endogenous GSH as ligands and cationic polymerized CS as a cross-linker and stabilizer.[99] The *in situ* synthesized CS–GSH@Au NCs exhibited SOD- and POD-like activities, facilitating the generation of H_2O_2 and $^{\bullet}OH$ from $O_2^{\bullet-}$. The authors mentioned that pristine glutathione-protected Au NCs possess POD-like activity, while the introduction of CS improves their SOD-like activity (Fig. 7h).

4. Biomedical application of metal NC-based artificial enzymes

Based on the enzyme-mimic catalytic behaviors, noble metal NCs have found potential applications in diverse fields, among which biomedical applications have attracted particular interest in the past years.[100,101] In this section, recent achievements in applying metal NCs in releasing oxidative stress and cancer detection/treatment will be deciphered, exemplifying the application potential of metal NCs in the biomedical field.

4.1 Treatment of oxidative stress disorders

Many diseases in living organisms are caused by inflammation, which occurs when the oxidative stress in living organisms is developed beyond the handling capability of their enzymes.[102] The extensive oxidative stress leads to the production of reactive oxygen species (ROS) that disrupt the organism's homeostatic balance. As over-accumulation of ROS in a prolonged period will significantly affect the organisms' health, it is highly desirable to develop biocompatible, efficient, and effective anti-oxidizing agents for releasing the *in vivo* oxidizing stress.

4.1.1 Acute kidney injury. Acute kidney injury (AKI) is a life-threatening disease characterized by prominent clinical features, including a rapid decline in renal excretion, decreased urine output, and increased nitrogen metabolism.[103] During AKI, excessive ROS/nitrogen species (RONS) react with biomolecules, triggering oxidative stress and inflammation, and further resulting in tubular necrosis and renal dysfunction, respectively. Recently, metal NCs have been used for the treatment of AKI, largely due to their ultra-small size (less than the renal clearance threshold of ~6 nm), which allows for timely excretion.[104] Besides the biosafety concerns, another root engine powers metal NCs' application in AKI is their enzyme-mimic catalytic activity, which contributes to eliminating excess ROS in the kidneys. Previous studies have demonstrated that nanoparticles smaller than 6 nm have a good ability to treat AKI. In 2021, Zhang *et al.* developed ~3 nm poly(vinylpyrrolidone)-coated platinum nanoparticles (Pt–PVP nanoparticles) as a multi-enzyme mimic (CAT, POD, and SOD). These Pt–PVP nanoparticles exhibited excellent scavenging capacity for ROS (such as $^{\bullet}OH$, $^{\bullet}O_2^-$ and H_2O_2) and effectively reduced POD-induced cellular damage[105] (Fig. 8a). In addition, Liu *et al.* successfully synthesized ultra-small $Cu_{5.4}O$ nanoparticles with multiple enzyme-mimic and broad-spectrum ROS scavenging activities.[106] These $Cu_{5.4}O$ nanoparticles exhibited combined catalytic performances of mimicking POD, SOD, and GPx. Due to their ultra-small size, $Cu_{5.4}O$ nanoparticles were rapidly cleared by the kidneys, ensuring their biocompatibility. Furthermore, even at very low doses, $Cu_{5.4}O$ nanoparticles demonstrated a cytoprotective effect against ROS-mediated injury, which can greatly inhibit

Published on 21 maart 2024. Downloaded on 10/11/2024 6:49:01.

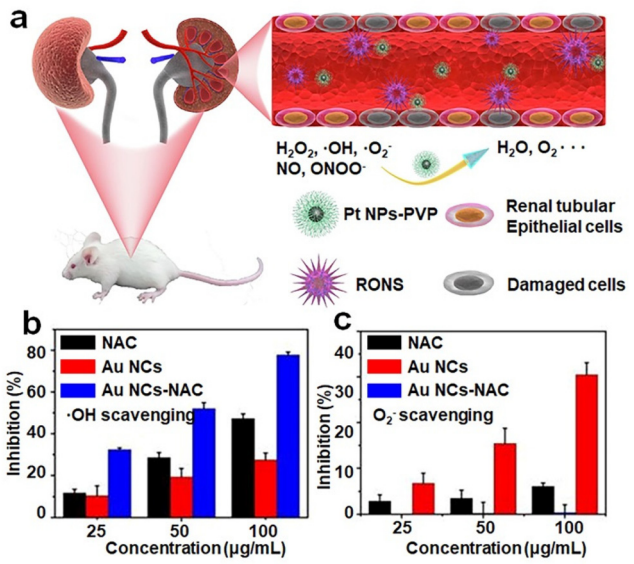

Fig. 8 (a) Schematic illustration of broad-spectrum antioxidant Pt-PVP nanoparticles for AKI treatment. Reproduced from ref. 105 with permission from Elsevier Sci Ltd, copyright 2020. (b) ˙OH radical and (c) $O_2^{\bullet-}$ radical-scavenging activity of NAC and Au NCs-NAC. Reproduced from ref. 95 with permission from Ivyspring International, copyright 2021.

AKI. Compared to nanoparticles, enzyme-mimic metal NCs with smaller size and higher catalytic activity offer a greater advantage in the treatment of AKI diseases. *N*-Acetylcysteine-capped Au NCs (Au NCs-NAC) have excellent POD-like and CAT-like activities, and can eliminate ˙OH and $O_2^{\bullet-}$ (Fig. 8b and c), offering a good mechanism to treat AKI diseases.[95]

4.1.2 Brain injury. Brain plays a central role in controlling the physical activities and metabolisms of organisms.[107] When the brain is damaged, it can critically impact the normal functioning of the organism. Inflammation is a common response to damage in the body and it requires the activation of enzymes largely by the brain to address the ROS components of inflammation. However, the brain itself becomes extremely vulnerable when it experiences inflammation, making the treatment of brain disorders more challenging.[108] Surgical interventions are often not feasible, making it tricky to address inflammatory responses within the brain. Nevertheless, the use of metal NCs in brain therapy has shown great potential. Metal NCs can afford several advantages: (1) they have high enzyme-mimic activity comparable to natural enzymes;[17] (2) they can potentially cross the blood–brain barrier (BBB) without the need for external forces like ultrasound;[109,110] and (3) the biocompatibility of the ligand used in metal NCs guarantees their safe use.[111] Since 2019, the Zhang group has conducted extensive research on the therapeutic effects of metal NCs on brain injury. They specifically focused on the therapeutic effects of different metal-doped Au_{25} NCs on neuroinflammation, as brain injury often leads to chronic inflammation. Fig. 9a schematically illustrates the inflammatory response associated with traumatic brain injury and the modulation of brain injury using $Au_{25}(MPA)_{18}$, $Au_{24}Cd_1(MPA)_{18}$, and $Au_{24}Cu_1(MPA)_{18}$ NCs, respectively. After the injury, it has witnessed an upregulation of interleukin-1β (IL-1β), interleukin-6 (IL-6), and tumor necrosis factor alpha (TNF-α), indicating a strong local inflammatory response.[112] It has been demonstrated that $Au_{24}Cd_1(MPA)_{18}$ and $Au_{24}Cu_1(MPA)_{18}$ NCs were effective in reducing the levels of the above-mentioned three inflammatory factors, suggesting that the substitution of Cu and Cd atoms significantly enhanced their catalytic activity (Fig. 9b). While $Au_{24}Cu_1(MPA)_{18}$ outperformed $Au_{24}Cd_1(MPA)_{18}$ in down-regulating TNF-α, $Au_{24}Cd_1(MPA)_{18}$ showed excellent performance in mediating the regulation of IL-1β and IL-6. In addition to Cu and Cd, doping Au_{25} NCs with Ag also greatly enhances their feasibility in treating oxidative stress and inflammatory responses[47] (Fig. 9c). *In vitro* modeling of oxidative stress with H_2O_2 and inflammation with lipopolysaccharide (LPS) demonstrated that $Au_{24}Ag_1(MPA)_{18}$ restored the H_2O_2-induced decrease with a cell viability of 93%, manifesting its potential neuroprotective effect (Fig. 9d). Fluorescence images revealed that excessive ROS, including $O_2^{\bullet-}$, ˙OH, and $^1O_2$, were present in the cells after H_2O_2 stimulation. However, the addition of $Au_{24}Ag_1(MPA)_{18}$ NCs reduced the ROS components, demonstrating their ability to scavenge free radicals *in vitro* and protect nerve cells (Fig. 9e).

Neurodegenerative diseases (NDDs), such as Parkinson's disease (PD), Alzheimer's disease (AD), and Huntington's disease (HD), are age-related diseases. In recent years, the prominence of NDDs has increased, with oxidative stress and the aggregation of α-syn proteins or Aβ proteins being important factors in their development.[113] The use of metal NCs for treating NDDs is currently limited to inhibiting the aggregation of pathogenic proteins[114] and research on the role of oxidative stress in NDD pathology has been stagnant. The main challenge lies in understanding how metal NCs are eliminated from the brain and the potential damage caused by their prolonged presence. Therefore, metal NC-assisted treatment of NDDs through the oxidative stress releasing mechanism represents a good topic for future study.

4.2 Tumor detection and treatment

Cancer is a globally recognized deadly disease of growing public concern.[115] Both timely detection and treatment of cancer are crucial for the survival of cancer patients. Metal NCs hold great potential in cancer detection and therapy due to the following reasons: (1) they possess abundant surface chemistry that can be utilized to conjugate the drug molecules or targeting molecules;[116] (2) their size is smaller than the renal clearance threshold value (6 nm), making metal NCs easy to be eliminated from the body and avoid cumulative damage;[117,118] (3) they exhibit good biocompatibility, exerting negligible harm to normal cells;[119] (4) they demonstrate good enzyme-mimic catalytic activity, facilitating the detection and treatment of cancer cells; (5) the discrete electron energy levels of metal NCs endowing them with unique optical properties,[120] such as NIR fluorescence,[121] enabling the detection

 This journal is © The Royal Society of Chemistry 2024

Published on 21 maart 2024. Downloaded on 10/11/2024 6:49:01.

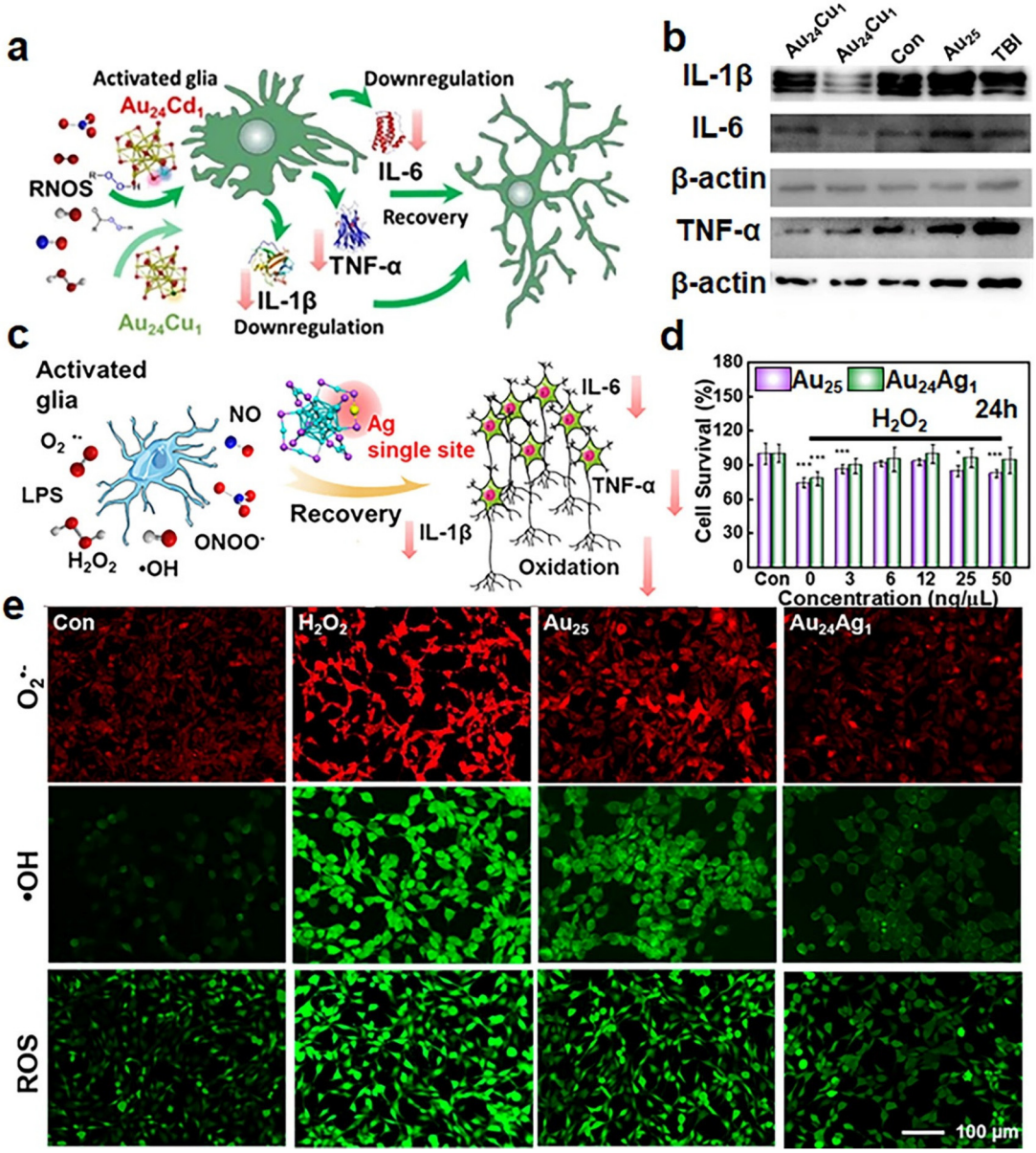

Fig. 9 (a) Schematic illustration of catalytic activity on the oxidative stress release and inflammatory responses of $Au_{24}Cd_1(MPA)_{18}$ and $Au_{24}Cu_1(MPA)_{18}$ NCs. (b) Expression levels of IL-1β, IL-6, and TNF-α in the brain tissues on day 30 post-TBI (traumatic brain injury) with or without clusters analyzed using western blotting. Reproduced from ref. 112 with permission from Springer, copyright 2021. (c) Schematic illustration of oxidative stress and inflammatory responses modulated using $Au_{24}Ag_1(MPA)_{18}$ after stimulation. (d) HT22 cell viability under H_2O_2 stimulation with $Au_{24}Ag_1(MPA)_{18}$ treatment. (e) Fluorescence images of $^{\bullet}OH$, $O_2^{\bullet-}$, and ROS with or without $Au_{24}Ag_1(MPA)_{18}$ treatment in H_2O_2-induced cells. Reproduced from ref. 47 with permission from American Chemical Society, copyright 2021.

of cancer sites;[122] and (6) metal NCs can afford multiple mechanisms, *e.g.*, photothermal,[123] radio-sensitizing,[124,125] and photodynamic[126,127] mechanisms, for killing cancer cells *in situ*.

4.2.1 Tumor detection. Early detection represents one of the most challenging issue in cancer theranostics.[128] *In vivo* detection of cancer is particularly challenging, as many conventional probing agents may trigger the immune response or hard to be cleared by the kidneys. Due to their small size, good biocompatibility, strong luminescence,[129–132] and excellent enzyme-mimic catalytic activity, metal NCs have emerged as a new family of diagnostic agents for various tumors. Au NCs with enzyme-mimicking properties were stabilized and coupled with a neutral fibrillar peptide (NAv), yielding Au NC–NAv complexes. In the detection process, the Au NC–NAv complex was administered intravenously and specifically cleaved by proteases at the lesion site. This cleavage resulted in the release of ultra-small-sized Au NCs, which were able to pass through the renal glomerulus and be excreted into the urine. Importantly, these Au NCs maintained their catalytic

Published on 21 maart 2024. Downloaded on 10/11/2024 6:49:01.

activity in the complex physiological environment. Therefore, the existence of tumor can be easily probed through the POD-like activity of Au NCs in the urine (Fig. 10a).[133] Au NCs can also be modified with positive-targeting molecules, like folic acid (FA), to realize their cancer detection applications. As shown in Fig. 10b, after conjugating Au NCs with FA, the Au NC–FA nanoprobes exhibited intense brown POD-like activity in the presence of a DAB (3,3′-diaminobenzidine) substrate and H_2O_2 in xenograft tumors, allowing positive tumor imaging *via* the fluorescence signals from the Au NC–FA nanoprobes.[134] This excellent performance can be utilized for immunohistochemistry (IHC) and immunofluorescence (IF) staining. Au NC–FA nanoprobes feature diverse advantages compared to conventional IHC and IF methods for staining cancer cell tissues, including shorter reaction times and simpler processing steps.

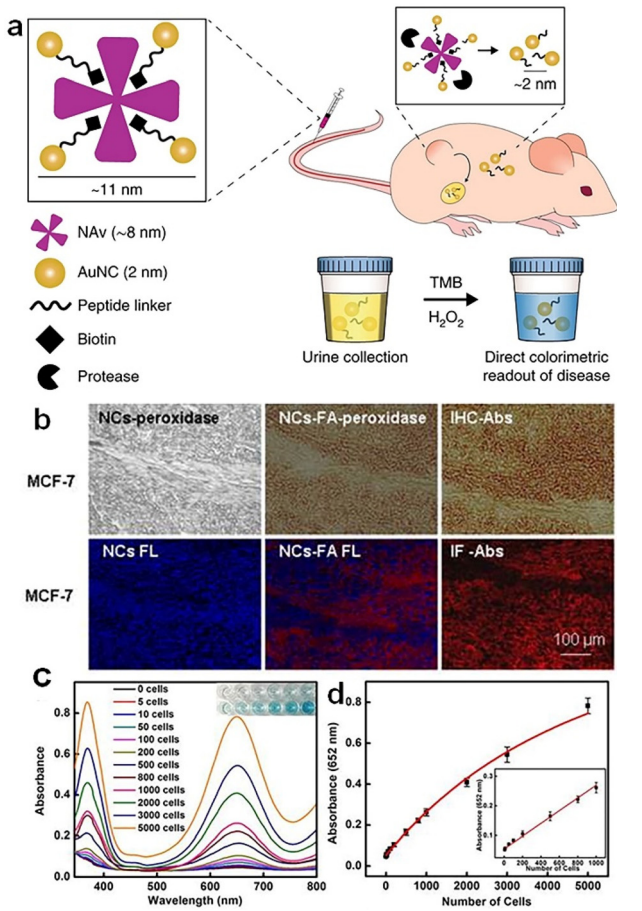

Fig. 10 (a) Schematic illustration of tumor detection based on Au NC–NAv complexes. Reproduced from ref. 133 with permission from Nature, copyright 2019. (b) MCF-7 tumor tissues stained with the Au NCs-FA nanoprobe and visualized by light microscopy and fluorescence (FL) microscopy, respectively. Reproduced from ref. 134 with permission from Ivyspring International, copyright 2014. (c) Absorbance spectra and visual color changes of MSN–AuNC–anti-HER2 solution in the presence of TMB and different numbers of SKBR3 cells. (d) Absorbance at 652 nm dependent on the number of SKBR3 cells. Reproduced from ref. 135 with permission from Ivyspring International, copyright 2014.

In addition to *in vivo* detection, blood testing offers a simple method for detecting cancer cells. Tao *et al.* conjugated silica–Au NC hybrids with HER2 antibody and developed a hybrid nanoprobe, MSN–AuNC–anti-HER2.[135] This nanoprobe enables the selective, quantitative, and rapid detection of HER2-positive breast cancer cells. The higher H_2O_2 content in cancer cells compared to normal cells allows Au NCs to catalyze the chromogenic reaction of H_2O_2 with substrates. In addition, the presence of HER2 antibodies enhances the specificity of MSN–AuNC–anti-HER2 in detecting HER2-positive breast cancer cells. As can be seen in Fig. 10c, the absorbance value increases with the number of SKBR3 cells. The absorbance of TMB at 652 nm shows a linear relationship with the number of target cancer cells, ranging from 5 to 1000 cells per mL, and the detection limit is as low as 5 cells per mL (Fig. 10d).

4.2.2 Tumor treatment. Cancer cells typically feature a higher H_2O_2 content in comparison with normal cells, which forms a basis for designing anti-cancer drugs.[136] Metal NCs can typically possess two types of therapeutic modes in H_2O_2-overloaded cancer cells. First, metal NCs can behave like POD and catalyze the decomposition of H_2O_2 into more oxidizing $^{\bullet}OH$ for effective killing of tumor cells. Second, as CAT mimics, metal NCs can facilitate the decomposition of H_2O_2 into O_2. The as-generated O_2 can be converted into ROS through radiotherapy or photothermal therapy for improving the killing efficiency of cancer cells. This mechanism is particularly important in the anaerobic microenvironment of cancer cells where oxygen is scarce. The conversion of H_2O_2 into $^{\bullet}OH$ in cancer cells, known as nanocatalytic therapy (NCT), has been explored as a potential method for eliminating cancer cells.[137] However, subsequent studies spotted out the deficiency of NCT in complete eradication of cancer cells. The root cause for this deficiency is that the conversion of endogenous H_2O_2 into $^{\bullet}OH$ in cancer cells is not sufficient to completely kill cancer cells. To address this limitation, researchers have adopted a combined therapy approach by incorporating photothermal therapy (PTT) and NCT. For instance, a novel alloy nanoenzyme, named DNA-Ag@Pd NC, possessing remarkable catalytic activity and superior NIR-II photothermal properties, was developed by simultaneously reducing Ag and Pd precursors in the presence of hairpin DNA structures as growth templates.[138] The nanoenzymes demonstrated outstanding NIR-II photothermal properties when exposed to 1270 nm laser irradiation (Fig. 11a). In addition, DNA-Ag@Pd NCs can effectively catalyze the oxidation of TMB with H_2O_2, indicating their high POD-like activity. Notably, DNA-Ag@Pd NCs exhibit significant POD-like activity within the pH range of 5.0–7.0, particularly at pH 5.0 presented by tumors (Fig. 11c). Mice experiments have demonstrated that DNA-Ag@Pd NCs, based on synergetic PTT and NCT mechanisms, can effectively eliminate tumor cells and inhibit tumor growth (Fig. 11d). In a separate contribution, Zhu *et al.* developed bimetallic $Pt_{50}Sn_{50}$ NCs with dual enzymatic activities, which exhibited enhanced POD-like and CAT-like activities under photothermal conditions.[139] The $Pt_{50}Sn_{50}$ NCs demonstrated significantly improved anticancer effects in multicellular tumor spheres and *in vivo* assays.

This journal is © The Royal Society of Chemistry 2024

Published on 21 maart 2024. Downloaded on 10/11/2024 6:49:01.

Metal NCs have also been employed as radiosensitizers in cancer radiotherapy, mostly due to the high atomic number of component metals. However, most previously reported metal NC-based radiosensitizers have a limited sensitizing effect, and are unable to overcome the radioresistance of hypoxic tumors. A practical approach to address this issue is promot-

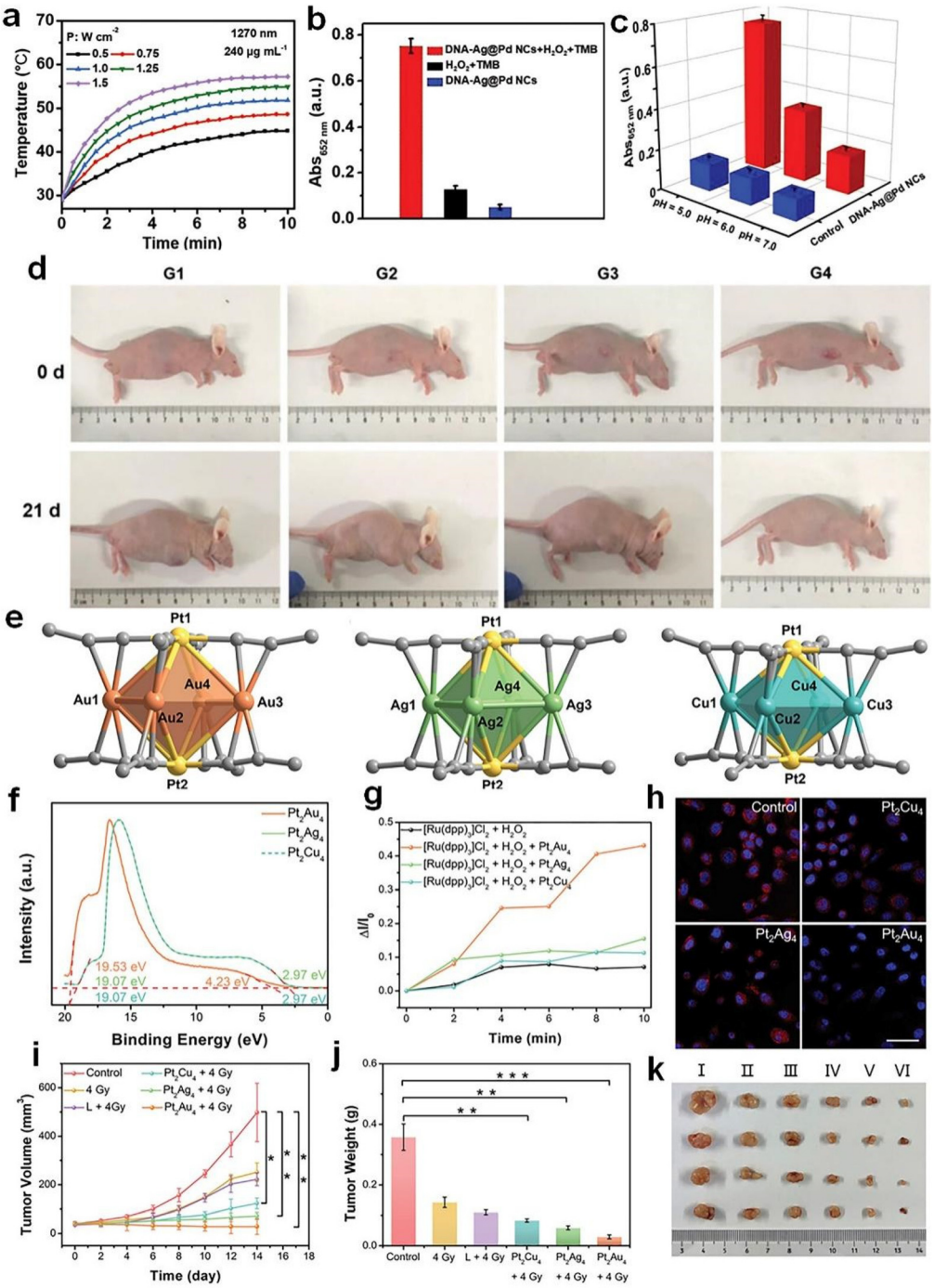

Fig. 11 (a) Photothermal heating curves of DNA–Ag@Pd NC aqueous suspensions under irradiation with a 1270 nm laser. (b) POD-like activity of DNA–Ag@Pd NCs. (c) Comparison of the POD-like activity of the blank group with DNA–Ag@Pd NCs at different pH values. (d) Photographs of the MKN-45-bearing mice before and after various treatments for 21 d. G1: PBS; G2: DNA-Ag@Pd NCs; G3: PBS + 1270 nm laser; G4: DNA-Ag@Pd NCs + 1270 nm laser. Reproduced from ref. 138 with permission from John Wiley and Sons, copyright 2023. (e) Structure, (f) ultraviolet photoelectron spectrum, and (g) time-dependent O_2 generation of $Pt_2Au_4(C_{21}H_{27}O_2)_8$, $Pt_2Ag_4(C_{21}H_{27}O_2)_8$, and $Pt_2Cu_4(C_{21}H_{27}O_2)_8$. (h) Confocal laser scanning microscopy (CLSM) images of intracellular O_2 generation under hypoxic conditions. (i) Tumor volume curves of mice after various treatments. (j) Statistical results of tumor weights in different groups. (k) Images of dissected tumors in: (I) control, (II) 4 Gy, (III) L + 4 Gy, (IV) $Pt_2Cu_4(C_{21}H_{27}O_2)_8$ + 4 Gy, (V) $Pt_2Ag_4(C_{21}H_{27}O_2)_8$ + 4 Gy, and (VI) $Pt_2Au_4(C_{21}H_{27}O_2)_8$ + 4 Gy groups. Reproduced from ref. 92 with permission from John Wiley and Sons, copyright 2022.

Published on 21 maart 2024. Downloaded on 10/11/2024 6:49:01.

ing fresh O_2 generation by *in situ* decomposition of over-expressed H_2O_2 in the tumor microenvironment, while such an H_2O_2 decomposition reaction can be catalyzed by using CAT-like metal NCs. Hua *et al.* prepared atomically precise alloy $Pt_2M_4(C_{21}H_{27}O_2)_8$ (M = Au, Ag, Cu) NCs with bright luminescence and good biocompatibility (Fig. 11e and f).[92] The synthesized $Pt_2Au_4(C_{21}H_{27}O_2)_8$ NCs exhibited excellent CAT-like activity and were able to convert H_2O_2 into O_2 in an anaerobic cellular environment (Fig. 11g and h). *In vivo* animal experiment showed that $Pt_2Au_4(C_{21}H_{27}O_2)_8$ NCs could generate a significant amount of more damaging ROS when exposed to X-rays under anaerobic conditions (Fig. 11i–k). Also, metal NCs with CAT-mimic activity can be used for the photodynamic therapy (PDT) of cancer cells. For example, polyamidoamine (PAMAM) dendrimer-encapsulated Au NCs have demonstrated optimal CAT-mimic activity within the physiological pH range[94] (*i.e.*, pH = 4.8–7.4). When combined with PDT for tumor treatment, it overcomes the oxygen deprivation of tumor cells, resulting in a better anticancer effect.

5. Conclusion

In this review, we discuss the hierarchical structures of metal NCs and their impact on enzyme-mimic catalytic activity. We also briefly review the current methods delivering atomically precise controllability on cluster structures at varied structural levels. Following the synthetic discussion, we summarize the diverse enzyme-mimic catalytic activities of metal NCs with an emphasis on principles governing them. Based on these enzyme-mimic catalytic activities, metal NCs have found potential applications in diverse fields of biomedicine, including the diagnosis and treatment of acute kidney injury, brain damage, and cancers. Despite the remarkable advances in the development of cluster chemistry, the development of metal NC-based artificial enzymes is still in its infancy. As nanochemistry is stepping into a new era of atomic precision, further development of atomically precise metal NCs as effective artificial enzymes requires combined efforts worldwide. Specific efforts may be devoted to the following topics in the near future.

Metal NCs, due to their molecule-like structure and properties, offer an ideal platform for unraveling the atomic-level structure–property relationship for metal-based artificial enzymes. However, there is a limited number of reports deciphering the interaction fundamentals of ROS with metal NCs at the atomic level. This is most probably due to the complex and dynamic surface structure of metal NCs, together with the fast reaction kinetics of ROS with metal NCs. Therefore, probing the dynamic reaction or interaction of ROS with metal NCs can be of core interest to the community.

While recent studies have shown that the catalytic effectiveness of many artificial enzymes can rival that of natural enzymes, the intricacy of living organisms lies in the fact that each enzyme serves a specific function. Aiming to develop metal NCs into an alternative or even better enzyme system to the natural ones, we may need to concentrate more on the catalytic selectivity in terms of both the reaction substrate and product. This is because current metal NC-based artificial enzymes can hardly exhibit catalytic selectivity comparable to that of natural enzymes. In addition to catalytic selectivity, future efforts may also be devoted to developing metal NC-based catalysts for cascade or tandem reactions, in which natural enzymes have shown their full potential.

Despite the rapid progress in the development and application of metal NCs with enzyme-mimic catalytic activity, there is still ongoing demand to explore their biocompatibility and/or toxicity mechanism to fully realize *in vivo* and clinical applications. The biocompatibility exploration may concern the immune responses caused by both the metal NCs themselves and their degradation products *in vivo*. Therefore, it is also important to understand the stabilization or degradation mechanism of metal NCs *in vivo*.

The application of NCs as mimetic enzymes in biomedicine extends beyond treating oxidative stress diseases and tumors. They also demonstrate positive effects in other biomedical areas like wound healing, bioimaging and so on. The versatile properties of NCs allow them to serve multiple functions in treatment processes. Often, there are synergistic effects from combining various treatment principles, such as radiotherapy and imaging, anti-inflammatory and antibacterial actions. This synergistic approach enhances the potential of metal NCs in biomedicine. Besides synergism in treating a single disease, the potential of treating multiple diseases with a single cluster has become a rising topic in the biomedical applications of metal NCs. This "one cluster for multiple purposes" approach aims to effectively address the challenges posed by complex diseases. Moreover, the exceptional water solubility of many metal NCs enables their use in spray or gel forms for treating certain skin conditions, which can definitively extend their scope of clinical applications. Overall, the versatile and unique properties of NCs may offer an alternative way to circumvent many long-existing challenges in the biomedical field.

Author contributions

Xinxin Pan: conceptualization and writing – original draft; Yidan Yao: writing – original draft; Manxi Zhang: writing – original draft; Xun Yuan: writing – review and editing; Qiaofeng Yao: supervision, funding acquisition, and writing – review and editing; Wenping Hu: supervision, funding acquisition, and writing – review and editing.

Conflicts of interest

There are no conflicts to declare.

Acknowledgements

The authors thankfully acknowledge the financial support from the National Natural Science Foundation of China

 This journal is © The Royal Society of Chemistry 2024

Published on 21 maart 2024. Downloaded on 10/11/2024 6:49:01.

(22371204) and the Fundamental Research Funds for the Central Universities.

References

1 R. Breslow and L. E. Overman, *J. Am. Chem. Soc.*, 1970, **92**, 1075–1077.
2 J. Suh and S. S. Hah, *J. Am. Chem. Soc.*, 1998, **120**, 10088–10093.
3 Y. Lin, J. Ren and X. Qu, *Adv. Mater.*, 2014, **26**, 4200–4217.
4 D. J. Mikolajczak, A. A. Berger and B. Koksch, *Angew. Chem., Int. Ed.*, 2020, **59**, 8776–8785.
5 Y. Lu, C. Cao, X. Pan, Y. Liu and D. Cui, *Nanoscale*, 2023, **15**, 14–40.
6 F. Manea, F. B. Houillon, L. Pasquato and P. Scrimin, *Angew. Chem., Int. Ed.*, 2004, **43**, 6165–6169.
7 L. Gao, J. Zhuang, L. Nie, J. Zhang, Y. Zhang, N. Gu, T. Wang, J. Feng, D. Yang, S. Perrett and X. Yan, *Nat. Nanotechnol.*, 2007, **2**, 577–583.
8 A. Asati, S. Santra, C. Kaittanis, S. Nath and J. M. Perez, *Angew. Chem., Int. Ed.*, 2009, **48**, 2308–2312.
9 J. E. Ghadiali and M. M. Stevens, *Adv. Mater.*, 2008, **20**, 4359–4363.
10 J. Xie, Y. Zheng and J. Y. Ying, *J. Am. Chem. Soc.*, 2009, **131**, 888–889.
11 H. Liu, Y. Li, S. Sun, Q. Xin, S. Liu, X. Mu, X. Yuan, K. Chen, H. Wang, K. Varga, W. Mi, J. Yang and X.-D. Zhang, *Nat. Commun.*, 2021, **12**, 114.
12 R. Jin, C. Zeng, M. Zhou and Y. Chen, *Chem. Rev.*, 2016, **116**, 10346–10413.
13 Q. Yao, T. Chen, X. Yuan and J. Xie, *Acc. Chem. Res.*, 2018, **51**, 1338–1348.
14 Q. Yao, L. Liu, S. Malola, M. Ge, H. Xu, Z. Wu, T. Chen, Y. Cao, M. F. Matus, A. Pihlajamäki, Y. Han, H. Häkkinen and J. Xie, *Nat. Chem.*, 2023, **15**, 230–239.
15 Q. Yao, Q. Zhang and J. Xie, *Ind. Eng. Chem. Res.*, 2022, **61**, 7594–7612.
16 H. Xu, D. Cheng, Y. Gao and X. C. Zeng, *ACS Catal.*, 2018, **8**, 9702–9710.
17 H. Shan, J. Shi, T. Chen, Y. Cao, Q. Yao, H. An, Z. Yang, Z. Wu, Z. Jiang and J. Xie, *ACS Nano*, 2023, **17**, 2368–2377.
18 Y. Pan, Z. Han, S. Chen, K. Wei and X. Wei, *Coord. Chem. Rev.*, 2023, **478**, 214964.
19 Y. Guo, H. T. N. N. Amunyela, Y. Cheng, Y. Xie, H. Yu, W. Yao, H.-W. Li and H. Qian, *Food Chem.*, 2021, **335**, 127657.
20 X. Kang, X. Wei, P. Xiang, X. Tian, Z. Zuo, F. Song, S. Wang and M. Zhu, *Chem. Sci.*, 2020, **11**, 4808–4816.
21 C. Kumara, K. Gagnon and A. Dass, *J. Phys. Chem. Lett.*, 2015, **6**, 1223–1228.
22 M. Bodiuzzaman, W. A. Dar and T. Pradeep, *Small*, 2021, **17**, 2003981.
23 Q. Yao, X. Yuan, T. Chen, D. T. Leong and J. Xie, *Adv. Mater.*, 2018, **30**, 1802751.
24 Y. Lei, Y. Wang, Y. Liu, C. Song, Q. Li, D. Wang and Y. Li, *Angew. Chem., Int. Ed.*, 2020, **59**, 20794–20812.
25 H. Bagheri, A. Afkhami, H. Khoshsafar, A. Hajian and A. Shahriyari, *Biosens. Bioelectron.*, 2017, **89**, 829–836.
26 B. Kumar, T. Kawawaki, N. Shimizu, Y. Imai, D. Suzuki, S. Hossain, L. V. Nair and Y. Negishi, *Nanoscale*, 2020, **12**, 9969–9979.
27 O. López-Estrada, N. Mammen, L. Laverdure, M. M. Melander, H. Häkkinen and K. Honkala, *ACS Catal.*, 2023, **13**, 8997–9006.
28 Y. Li, S. Li, A. V. Nagarajan, Z. Liu, S. Nevins, Y. Song, G. Mpourmpakis and R. Jin, *J. Am. Chem. Soc.*, 2021, **143**, 11102–11108.
29 G. Hu, Z. Wu and D.-e. Jiang, *J. Mater. Chem. A*, 2018, **6**, 7532–7537.
30 H. Seong, M. Choi, S. Park, H.-w. Kim, J. Kim, W. Kim, J. S. Yoo and D. Lee, *ACS Energy Lett.*, 2022, **7**, 4177–4184.
31 H. Seong, V. Efremov, G. Park, H. Kim, J. S. Yoo and D. Lee, *Angew. Chem., Int. Ed.*, 2021, **60**, 14563–14570.
32 L. Qin, G. Ma, L. Wang and Z. Tang, *J. Energy Chem.*, 2021, **57**, 359–370.
33 J. Zhao, A. Ziarati, A. Rosspeintner and T. Bürgi, *Angew. Chem., Int. Ed.*, 2024, **63**, e202316649.
34 X. Ma, F. Sun, L. Qin, Y. Liu, X. Kang, L. Wang, D.-e. Jiang, Q. Tang and Z. Tang, *Chem. Sci.*, 2022, **13**, 10149–10158.
35 X. Cai, G. Li, W. Hu and Y. Zhu, *ACS Catal.*, 2022, **12**, 10638–10653.
36 L. Tang, Y. Luo, X. Ma, B. Wang, M. Ding, R. Wang, P. Wang, Y. Pei and S. Wang, *Angew. Chem., Int. Ed.*, 2023, **62**, e202300553.
37 S. Wang, S. Jin, S. Yang, S. Chen, Y. Song, J. Zhang and M. Zhu, *Sci. Adv.*, 2015, **1**, e1500441.
38 Y. Yun, H. Sheng, K. Bao, L. Xu, Y. Zhang, D. Astruc and M. Zhu, *J. Am. Chem. Soc.*, 2020, **142**, 4126–4130.
39 Y. Jv, B. Li and R. Cao, *Chem. Commun.*, 2010, **46**, 8017–8019.
40 M. Sharifi, K. Faryabi, A. J. Talaei, M. S. Shekha, M. Ale-Ebrahim, A. Salihi, N. M. Q. Nanakali, F. M. Aziz, B. Rasti, A. Hasan and M. Falahati, *J. Mol. Liq.*, 2020, **297**, 112004.
41 R. López-Domene, S. Vázquez-Díaz, E. Modin, A. Beloqui and A. L. Cortajarena, *Adv. Funct. Mater.*, 2023, **33**, 2301131.
42 S. Back, M. S. Yeom and Y. Jung, *ACS Catal.*, 2015, **5**, 5089–5096.
43 M. S. Bootharaju, C. P. Joshi, M. R. Parida, O. F. Mohammed and O. M. Bakr, *Ind. Eng. Chem. Res.*, 2016, **55**, 922–926.
44 A. G. Walsh and P. Zhang, *Adv. Mater. Interfaces*, 2021, **8**, 2001342.
45 Y. Shichibu, F. Zhang, Y. Chen, M. Konishi, S. Tanaka, H. Imoto, K. Naka and K. Konishi, *J. Chem. Phys.*, 2021, **155**, 054301.
46 K. Kwak, W. Choi, Q. Tang, M. Kim, Y. Lee, D.-e. Jiang and D. Lee, *Nat. Commun.*, 2017, **8**, 14723.
47 S. Sun, H. Liu, Q. Xin, K. Chen, H. Ma, S. Liu, X. Mu, W. Hao, S. Liu, Y. Gao, Y. Wang, J. Pei, R. Zhao, S. Zhang,

Published on 21 maart 2024. Downloaded on 10/11/2024 6:49:01.

X. Zhang, H. Wang, Y. Li and X.-D. Zhang, *Nano Lett.*, 2021, **21**, 2562–2571.
48 Y. Chen, C. Liu, Q. Tang, C. Zeng, T. Higaki, A. Das, D.-e. Jiang, N. L. Rosi and R. Jin, *J. Am. Chem. Soc.*, 2016, **138**, 1482–1485.
49 R. R. Nasaruddin, T. Chen, J. Li, N. Goswami, J. Zhang, N. Yan and J. Xie, *ChemCatChem*, 2018, **10**, 395–402.
50 J.-Q. Wang, R.-L. He, W.-D. Liu, Q.-Y. Feng, Y.-E. Zhang, C.-Y. Liu, J.-X. Ge and Q.-M. Wang, *J. Am. Chem. Soc.*, 2023, **145**, 12255–12263.
51 J. W. Padelford, M. Zhou, Y. Chen, R. Jin and G. Wang, *J. Phys. Chem. C*, 2017, **121**, 21217–21224.
52 L. Liao, S. Zhou, Y. Dai, L. Liu, C. Yao, C. Fu, J. Yang and Z. Wu, *J. Am. Chem. Soc.*, 2015, **137**, 9511–9514.
53 J. Yu, S. Choi and R. M. Dickson, *Angew. Chem., Int. Ed.*, 2009, **48**, 318–320.
54 T. Jia, Z.-J. Guan, C. Zhang, X.-Z. Zhu, Y.-X. Chen, Q. Zhang, Y. Yang and D. Sun, *J. Am. Chem. Soc.*, 2023, **145**, 10355–10363.
55 X. Ma, Z. Tang, L. Qin, J. Peng, L. Li and S. Chen, *Nanoscale*, 2020, **12**, 2980–2986.
56 P. Bose, K. Kumaranchira Ramankutty, P. Chakraborty, E. Khatun and T. Pradeep, *Nanoscale*, 2024, **16**, 1446–1470.
57 Z. Wang, X. Pan, S. Qian, G. Yang, F. Du and X. Yuan, *Coord. Chem. Rev.*, 2021, **438**, 213900.
58 R. R. Nasaruddin, T. Chen, N. Yan and J. Xie, *Coord. Chem. Rev.*, 2018, **368**, 60–79.
59 Y. Zaker, B. A. Ashenfelter, B. Bhattarai, N. A. Diemler, T. R. Brewer and T. P. Bigioni, *Small*, 2021, **17**, 2002238.
60 Y.-F. Lin, C.-R. Yang, Y.-F. Huang and H.-T. Chang, *J. Chin. Chem. Soc.*, 2022, **69**, 1200–1209.
61 L. Tang, A. Ma, C. Zhang, X. Liu, R. Jin and S. Wang, *Angew. Chem., Int. Ed.*, 2021, **60**, 17969–17973.
62 Y. Song, T. Cao, H. Deng, X. Zhu, P. Li and M. Zhu, *Sci. China: Chem.*, 2014, **57**, 1218–1224.
63 S. Chen, S. Wang, J. Zhong, Y. Song, J. Zhang, H. Sheng, Y. Pei and M. Zhu, *Angew. Chem., Int. Ed.*, 2015, **54**, 3145–3149.
64 W. Du, S. Jin, L. Xiong, M. Chen, J. Zhang, X. Zou, Y. Pei, S. Wang and M. Zhu, *J. Am. Chem. Soc.*, 2017, **139**, 1618–1624.
65 B. M. Barngrover and C. M. Aikens, *J. Am. Chem. Soc.*, 2012, **134**, 12590–12595.
66 Y. Li, O. Zaluzhna, B. Xu, Y. Gao, J. M. Modest and Y. J. Tong, *J. Am. Chem. Soc.*, 2011, **133**, 2092–2095.
67 X. Yuan, B. Zhang, Z. Luo, Q. Yao, D. T. Leong, N. Yan and J. Xie, *Angew. Chem., Int. Ed.*, 2014, **53**, 4623–4627.
68 Z. Luo, V. Nachammai, B. Zhang, N. Yan, D. T. Leong, D.-e. Jiang and J. Xie, *J. Am. Chem. Soc.*, 2014, **136**, 10577–10580.
69 Q. Yao, X. Yuan, V. Fung, Y. Yu, D. T. Leong, D. E. Jiang and J. Xie, *Nat. Commun.*, 2017, **8**, 927.
70 L. M. Tvedte and C. J. Ackerson, *J. Phys. Chem. A*, 2014, **118**, 8124–8128.
71 Y. Shichibu, Y. Negishi, H. Tsunoyama, M. Kanehara, T. Teranishi and T. Tsukuda, *Small*, 2007, **3**, 835–839.
72 Y. Cao, T. Liu, T. Chen, B. Zhang, D.-e. Jiang and J. Xie, *Nat. Commun.*, 2021, **12**, 3212.
73 Y. Shichibu, Y. Negishi, T. Tsukuda and T. Teranishi, *J. Am. Chem. Soc.*, 2005, **127**, 13464–13465.
74 L. G. AbdulHalim, N. Kothalawala, L. Sinatra, A. Dass and O. M. Bakr, *J. Am. Chem. Soc.*, 2014, **136**, 15865–15868.
75 Q. Yao, Y. Feng, V. Fung, Y. Yu, D.-e. Jiang, J. Yang and J. Xie, *Nat. Commun.*, 2017, **8**, 1555.
76 Y. Cao, S. Malola, M. F. Matus, T. Chen, Q. Yao, R. Shi, H. Häkkinen and J. Xie, *Chem*, 2021, **7**, 2227–2244.
77 J. Yan, B. K. Teo and N. Zheng, *Acc. Chem. Res.*, 2018, **51**, 3084–3093.
78 F. K. de Oliveira, L. O. Santos and J. G. Buffon, *Food Res. Int.*, 2021, **143**, 110266.
79 S. Wang, W. Chen, A. L. Liu, L. Hong, H. H. Deng and X. H. Lin, *ChemPhysChem*, 2012, **13**, 1199–1204.
80 J. Li, W. Liu, X. Wu and X. Gao, *Biomaterials*, 2015, **48**, 37–44.
81 X. Jiang, C. Sun, Y. Guo, G. Nie and L. Xu, *Biosens. Bioelectron.*, 2015, **64**, 165–170.
82 L. Jin, Z. Meng, Y. Zhang, S. Cai, Z. Zhang, C. Li, L. Shang and Y. Shen, *ACS Appl. Mater. Interfaces*, 2017, **9**, 10027–10033.
83 S. Maity, D. Bain, S. Chakraborty, S. Kolay and A. Patra, *ACS Sustainable Chem. Eng.*, 2020, **8**, 18335–18344.
84 V. Mora-Sanz, L. Saa, N. Briz and V. Pavlov, *Chem. Mater.*, 2020, **32**, 8286–8293.
85 Y. Tao, Y. Lin, Z. Huang, J. Ren and X. Qu, *Adv. Mater.*, 2013, **25**, 2594–2599.
86 Z.-F. Pu, J. Peng, Q.-L. Wen, Y. Li, J. Ling, P. Liu and Q.-E. Cao, *Dyes Pigm.*, 2021, **193**, 109533.
87 M. Alfonso-Prieto, X. Biarnés, P. Vidossich and C. Rovira, *J. Am. Chem. Soc.*, 2009, **131**, 11751–11761.
88 C. Zhang, X. Wang, J. Du, Z. Gu and Y. Zhao, *Adv. Sci.*, 2021, **8**, 2002797.
89 M. Kajita, K. Hikosaka, M. Iitsuka, A. Kanayama, N. Toshima and Y. Miyamoto, *Free Radic. Res.*, 2009, **41**, 615–626.
90 H. Ma, X. Zhang, L. Liu, Y. Huang, S. Sun, K. Chen, Q. Xin, P. Liu, Y. Yan, Y. Wang, Y. Li, H. Liu, R. Zhao, K. Tan, X. Chen, X. Yuan, Y. Li, Y. Liu, H. Dai, C. Liu, H. Wang and X.-D. Zhang, *Sci. Adv.*, 2023, **9**, eadh7828.
91 M. Jiao, X. Mu, S. Sun, H. Yang, L. Ouyang, S. Zhang, J. Guo, J. Meng, Y. Liu, H. Ma, H. Wang, J. Pei, R. Zhao, T. Liu, W. Long, X.-D. Zhang and R. Zhang, *Chem. Eng. J.*, 2022, **445**, 136793.
92 Y. Hua, J.-H. Huang, Z.-H. Shao, X.-M. Luo, Z.-Y. Wang, J.-Q. Liu, X. Zhao, X. Chen and S.-Q. Zang, *Adv. Mater.*, 2022, **34**, 2203734.
93 C. Liu, Y. Cai, J. Wang, X. Liu, H. Ren, L. Yan, Y. Zhang, S. Yang, J. Guo and A. Liu, *ACS Appl. Mater. Interfaces*, 2020, **12**, 42521–42530.
94 C. P. Liu, T. H. Wu, Y. L. Lin, C. Y. Liu, S. Wang and S. Y. Lin, *Small*, 2016, **12**, 4127–4135.

 This journal is © The Royal Society of Chemistry 2024

Published on 21 maart 2024. Downloaded on 10/11/2024 6:49:01.

95 D.-Y. Zhang, T. Tu, M. R. Younis, K. S. Zhu, H. Liu, S. Lei, J. Qu, J. Lin and P. Huang, *Theranostics*, 2021, **11**, 9904–9917.
96 Q. Dan, D. Hu, Y. Ge, S. Zhang, S. Li, D. Gao, W. Luo, T. Ma, X. Liu, H. Zheng, Y. Li and Z. Sheng, *Biomater. Sci.*, 2020, **8**, 973–987.
97 P. Saxena, K. Selvaraj, S. K. Khare and N. Chaudhary, *Biotechnol. Lett.*, 2022, **44**, 1–22.
98 M. Kajita, K. Hikosaka, M. Iitsuka, A. Kanayama, N. Toshima and Y. Miyamoto, *Free Radic. Res.*, 2007, **41**, 615–626.
99 W. Mi, S. Tang, S. Guo, H. Li and N. Shao, *Chin. Chem. Lett.*, 2022, **33**, 1331–1336.
100 Y. Zhang, S. Li, H. Liu, W. Long and X. D. Zhang, *Front. Chem.*, 2020, **8**, 219.
101 F. Sun, Y. Liang, L. Jin, J. Shi and L. Shang, *ACS Appl. Mater. Interfaces*, 2021, **13**, 58209–58219.
102 K. Li, D. Li, C.-H. Li, P. Zhuang, C. Dai, X. Hu, D. Wang, Y. Liu, X. Mei and V. M. Rotello, *Nanoscale*, 2021, **13**, 6531–6537.
103 J. A. Kellum, P. Romagnani, G. Ashuntantang, C. Ronco, A. Zarbock and H.-J. Anders, *Nat. Rev. Dis. Primers*, 2021, **7**, 52.
104 S. Li, N. Yang, Q. Ma, S. Li, S. Tong, J. Luo, X. Song and H. Yang, *Anal. Chem.*, 2023, **95**, 16153–16159.
105 D.-Y. Zhang, H. Liu, M. R. Younis, S. Lei, C. Yang, J. Lin, J. Qu and P. Huang, *Chem. Eng. J.*, 2021, **409**, 127371.
106 T. Liu, B. Xiao, F. Xiang, J. Tan, Z. Chen, X. Zhang, C. Wu, Z. Mao, G. Luo, X. Chen and J. Deng, *Nat. Commun.*, 2020, **11**, 2788.
107 P. D. Loprinzi, S. M. Herod, B. J. Cardinal and T. D. Noakes, *Brain Res.*, 2013, **1539**, 95–104.
108 N. E. Gilhus and G. Deuschl, *Nat. Rev. Neurosci.*, 2019, **15**, 429–430.
109 J. Hu, G. Gao, M. He, Q. Yin, X. Gao, H. Xu and T. Sun, *Nanomedicine*, 2020, **15**, 563–580.
110 X. Pan, Z. Zuo, Z. Wang, G. Yang, H. Zhu, Y. Li and X. Yuan, *Mater. Chem. Front.*, 2023, **7**, 1146–1152.
111 Y. Zheng, J. Wu, H. Jiang and X. Wang, *Coord. Chem. Rev.*, 2021, **431**, 213689.
112 Y. Zhang, S. Sun, H. Liu, Q. Ren, W. Hao, Q. Xin, J. Xu, H. Wang and X.-D. Zhang, *J. Nanobiotechnol.*, 2021, **19**, 319.
113 D. M. Wilson, M. R. Cookson, L. Van Den Bosch, H. Zetterberg, D. M. Holtzman and I. Dewachter, *Cell*, 2023, **186**, 693–714.
114 G. Gao, R. Chen, M. He, J. Li, J. Li, L. Wang and T. Sun, *Biomaterials*, 2019, **194**, 36–46.
115 R. Bernards, E. Jaffee, J. A. Joyce, S. W. Lowe, E. R. Mardis, S. J. Morrison, K. Polyak, C. L. Sears, K. H. Vousden and Z. Zhang, *Nat. Cancer*, 2020, **1**, 12–17.
116 A. Yahia-Ammar, D. Sierra, F. Mérola, N. Hildebrandt and X. Le Guével, *ACS Nano*, 2016, **10**, 2591–2599.
117 G. Yang, Z. Wang, F. Du, F. Jiang, X. Yuan and J. Y. Ying, *J. Am. Chem. Soc.*, 2023, **145**, 11879–11898.
118 J. Liu, M. Yu, C. Zhou and J. Zheng, *Mater. Today*, 2013, **16**, 477–486.
119 J. Liu, M. Yu, C. Zhou, S. Yang, X. Ning and J. Zheng, *J. Am. Chem. Soc.*, 2013, **135**, 4978–4981.
120 Y. Zeng, S. Havenridge, M. Gharib, A. Baksi, K. L. D. M. Weerawardene, A. R. Ziefuß, C. Strelow, C. Rehbock, A. Mews, S. Barcikowski, M. M. Kappes, W. J. Parak, C. M. Aikens and I. Chakraborty, *J. Am. Chem. Soc.*, 2021, **143**, 9405–9414.
121 D. Li, Q. Liu, Q. Qi, H. Shi, E.-C. Hsu, W. Chen, W. Yuan, Y. Wu, S. Lin, Y. Zeng, Z. Xiao, L. Xu, Y. Zhang, T. Stoyanova, W. Jia and Z. Cheng, *Small*, 2020, **16**, 2003851.
122 Y. Tao, Y. Lin, Z. Huang, J. Ren and X. Qu, *Adv. Mater.*, 2013, **25**, 2594–2599.
123 G. Yang, X. Mu, X. Pan, Y. Tang, Q. Yao, Y. Wang, F. Jiang, F. Du, J. Xie, X. Zhou and X. Yuan, *Chem. Sci.*, 2023, **14**, 4308–4318.
124 X. D. Zhang, J. Chen, Z. Luo, D. Wu, X. Shen, S. S. Song, Y. M. Sun, P. X. Liu, J. Zhao, S. Huo, S. Fan, F. Fan, X. J. Liang and J. Xie, *Adv. Healthcare Mater.*, 2014, **3**, 133–141.
125 Y. Chen, J. Yang, S. Fu and J. Wu, *Int. J. Nanomed.*, 2020, **15**, 9407–9430.
126 R. Han, M. Zhao, Z. Wang, H. Liu, S. Zhu, L. Huang, Y. Wang, L. Wang, Y. Hong, Y. Sha and Y. Jiang, *ACS Nano*, 2020, **14**, 9532–9544.
127 P. Huang, J. Lin, S. Wang, Z. Zhou, Z. Li, Z. Wang, C. Zhang, X. Yue, G. Niu, M. Yang, D. Cui and X. Chen, *Biomaterials*, 2013, **34**, 4643–4654.
128 R. C. Fitzgerald, A. C. Antoniou, L. Fruk and N. Rosenfeld, *Nat. Med.*, 2022, **28**, 666–677.
129 S. Chen, W. Du, C. Qin, D. Liu, L. Tang, Y. Liu, S. Wang and M. Zhu, *Angew. Chem., Int. Ed.*, 2020, **59**, 7542–7547.
130 X. Wang, B. Yin, L. Jiang, C. Yang, Y. Liu, G. Zou, S. Chen and M. Zhu, *Science*, 2023, **381**, 784–790.
131 X. Wei, X. Kang, Z. Zuo, F. Song, S. Wang and M. Zhu, *Natl. Sci. Rev.*, 2020, **8**, 4018–4021.
132 S. Wang, X. Meng, A. Das, T. Li, Y. Song, T. Cao, X. Zhu, M. Zhu and R. Jin, *Angew. Chem., Int. Ed.*, 2014, **53**, 2376–2380.
133 C. N. Loynachan, A. P. Soleimany, J. S. Dudani, Y. Lin, A. Najer, A. Bekdemir, Q. Chen, S. N. Bhatia and M. M. Stevens, *Nat. Nanotechnol.*, 2019, **14**, 883–890.
134 D. Hu, Z. Sheng, S. Fang, Y. Wang, D. Gao, P. Zhang, P. Gong, Y. Ma and L. Cai, *Theranostics*, 2014, **4**, 142–153.
135 Y. Tao, M. Li, B. Kim and D. T. Auguste, *Theranostics*, 2017, **7**, 899–911.
136 C. Shen, T. Jiang, Q. Lou, W. Zhao, C. Lv, G. Zheng, H. Liu, P. Li, L. Dai, K. Liu, J. Zang, F. Wang, L. Dong, S. Qu, Z. Cheng and C. Shan, *SmartMat*, 2022, **3**, 269–285.
137 Z. Tang, Y. Liu, M. He and W. Bu, *Angew. Chem., Int. Ed.*, 2019, **58**, 946–956.
138 Y. Zhang, Y. Li, J. Li, F. Mu, J. Wang, C. Shen, H. Wang, F. Huang, B. Chen, Z. Luo and L. Wang, *Adv. Healthcare Mater.*, 2023, **12**, e2300267.
139 Y. Zhu, R. Zhao, L. Feng, C. Wang, S. Dong, M. V. Zyuzin, A. Timin, N. Hu, B. Liu and P. Yang, *ACS Nano*, 2023, **17**, 6833–6848.